Simulations of primary and secondary ice production during an Arctic mixed-phase cloud case from the NASCENT campaign

Britta Schäfer[1], Robert Oscar David[1], Paraskevi Georgakaki[2], Julie Pasquier[3], Georgia Sotiropoulou[4,2], and Trude Storelvmo[1,5]

[1]University of Oslo, Postbox 1022, Blindern, 0315 Oslo, Norway
[2]Laboratory of Atmospheric Processes and their Impacts, School of Architecture, Civil and Environmental Engineering, École Polytechnique Fédérale de Lausanne, Lausanne 1015, Switzerland
[3]Meteomatics AG, St. Gallen, Switzerland
[4]National and Kapodistrian University of Athens, Greece
[5]Nord University, Bodø, Norway

Correspondence: Britta Schäfer (britta.schafer@geo.uio.no)

Abstract. The Arctic is the fastest warming environment on Earth and the role of clouds in this warming is undisputed. The representation of Arctic clouds and their phase distribution, i.e. the amount of ice and supercooled water, influences predictions of future Arctic warming. Therefore, it is essential that cloud phase is correctly captured by models in order to accurately predict the future Arctic climate. Ice crystal formation in clouds happens through ice nucleation (primary ice production) and

5   ice multiplication (secondary ice production). In common weather and climate models, rime-splintering is the only secondary ice production process included. In addition, prescribed number concentrations of cloud condensation nuclei or cloud droplets and ice-nucleating particles are often overestimated in Arctic environments by standard model configurations. This can lead to a misrepresentation of the phase distribution and precipitation formation in Arctic mixed-phase clouds, with important implications for the Arctic surface energy budget. During the Ny-Ålesund Aerosol Cloud Experiment (NASCENT) a holographic

10   probe mounted on a tethered balloon took in-situ measurements of ice crystal and cloud droplet number and mass concentrations in Svalbard, Norway, during fall 2019 and spring 2020. In this study, we choose one case study from this campaign showing evidence of strong secondary ice production and use the Weather Research and Forecasting (WRF) model to simulate it at a high vertical and spatial resolution. We test the performance of different microphysical parametrizations and apply a new state-of-the-art secondary ice parametrization. We find that the agreement with observations highly depends on the prescribed

15   cloud condensation nuclei/cloud droplet and ice-nucleating particle concentration and requires an enhancement of secondary ice production processes. Lowering mass mixing ratio thresholds for rime splintering inside the Morrison microphysics scheme is crucial for enabling secondary ice production and thereby matching observations for the right reasons. The latter is a prerequisite for reliable simulations of Arctic mixed-phase cloud responses to future temperature- or aerosol perturbations.

1 Introduction

As the fastest warming region on Earth, the Arctic is of special interest for climate research and particular efforts are made to understand the role of clouds in this region (e.g. Serreze and Barry, 2011; Wendisch et al., 2017, 2019). Cloud phase is an important parameter in Arctic clouds as it influences both their radiative properties and lifetime, and thereby controls their climatic impact (e.g. Morrison et al., 2012). Mixed-phase clouds, i.e. clouds consisting of both ice crystals and supercooled

25 liquid water droplets, can form at temperatures between approximately -38 and 0 °C. In the Arctic, these clouds frequently occur in every season and are especially common at low and mid-levels (Shupe et al., 2006; de Boer et al., 2009; Shupe, 2011; Gierens et al., 2020). In order for ice to form in the mixed-phase cloud temperature regime, a special subset of aerosol known as ice-nucleating particles (INPs) is required. INPs act as a catalyst for water to freeze at temperatures above -38 °C (the homogeneous freezing temperature of water, Vali et al. (2015)). Previous studies suggest that ice formation and thereby also the

30 phase partitioning between liquid and ice are strongly affected by the availability of INPs (Jackson et al., 2012; Solomon et al., 2018; Norgren et al., 2018; Carlsen and David, 2022; Creamean et al., 2022). However, to which degree the phase composition is determined by INPs is still an ongoing topic of research and investigated in field campaigns (e.g. Pasquier et al., 2022a).

There are different mechanisms through which INPs can nucleate ice, namely immersion, contact, condensation and deposition freezing (Vali et al., 2015). Immersion freezing occurs when an INP is immersed in a liquid droplet and initiates freezing (Vali

35 et al., 2015). Condensation freezing is similar to immersion freezing except that the INP acts as a cloud condensation nuclei (CCN) and nucleates ice as soon as bulk water condenses on its surface. Contact freezing occurs when an INP triggers a supercooled cloud droplet to freeze upon collision (Diehl et al., 2002; Yang et al., 2020). Lastly, deposition freezing occurs when water vapor directly nucleates into ice on an INP (Vali et al., 2015), however more recent studies have shown that deposition freezing may actually occur due to bulk water condensed in nano-scale cracks or pores i.e. pore condensation and freezing (e.g.

40 David et al., 2019b, 2020; Marcolli, 2014; Campbell and Christenson, 2018). Although condensation freezing is considered a separate ice nucleation process, it is debatable whether it is microphysically different from deposition/pore condensation and freezing and immersion freezing (Kanji et al., 2017).

While these heterogeneous ice nucleation processes together with homogeneous nucleation are commonly summarized as primary ice production processes, there has long been evidence for the existence of additional processes enhancing the number of

45 ice crystals in clouds. Field measurements show that ice crystal number concentrations (ICNC) can significantly exceed INP concentrations (INPC) in clouds by up to five orders of magnitude (e.g. Auer et al., 1969; Beard, 1992; Cantrell and Heymsfield, 2005; Korolev and Leisner, 2020; Wieder et al., 2022a). To explain this discrepancy, a number of so-called secondary ice production (SIP) processes for the multiplication of ice from existing frozen particles have been proposed. These processes include the collisional breakup of ice crystals (BR), rime splintering (RS, also called Hallett-Mossop process), droplet shatter-

50 ing when freezing (DS) and sublimation fragmentation in subsaturated cloud regions (SF) (e.g. Field et al., 2017; Korolev and Leisner, 2020). RS occurs when liquid droplets (diameter < 13 μm) or drops (>25 μm) rime on ice crystals but is only believed to be active in the temperature range between -8 °C and -3 °C (Hallett and Mossop, 1974; Mossop, 1978; Field et al., 2017). BR, caused by ice-ice collisions, and DS, i.e. splinter production during the freezing of large droplets, as well as SF have been

observed outside of this temperature range (Lauber et al., 2018; Korolev and Leisner, 2020; Keinert et al., 2020; Lauber et al.,
55 2021, and references therein), and thus, have the potential to significantly increase ICNC throughout the entire mixed-phase
temperature range (Karalis et al., 2022).

Nevertheless, RS is generally the only SIP process that is part of standard microphysics schemes available for both numerical
weather prediction and climate models (e.g. Field et al., 2017; Zhao et al., 2021; Atlas et al., 2022). Many previous studies of
model-observation comparisons therefore do not include additional SIP processes (Prenni et al., 2007; Luo et al., 2008; Barton
60 et al., 2012; Young et al., 2017; Schemann and Ebell, 2020). These include e.g. the extensive modeling of Arctic stratocumulus
clouds performed by Solomon et al. (2009) for cases from the M-PACE campaign that took place in 2004 (Verlinde et al.,
2007). They tested several one- and two-moment schemes, all without SIP apart from RS, inside the Weather Research and
Forecasting model (WRF) (Skamarock et al., 2019), and found an underestimation of the number of small ice crystals. How-
ever, more recent studies have started including DS and BR to address the lack of SIP processes in models. E.g., Fu et al. (2019)
65 studied a case from the same campaign using the Milbrandt and Yau microphysics scheme (Milbrandt and Yau, 2005) with
different SIP configurations including tests for DS and BR. They found that BR did not contribute significantly in their case
while DS enhanced ICNC by roughly a factor of 2. Also, Sotiropoulou et al. (2021) and Georgakaki et al. (2022) implemented
BR and DS, respectively, into the Morrison microphysics scheme (Morrison et al., 2009) in the WRF model following the
parametrizations by Phillips et al. (2017, 2018). Sotiropoulou et al. (2021) found that including BR improved the representa-
70 tion of ICNC in the model considerably compared to field observations of Antarctic clouds. Georgakaki et al. (2022) found that
including BR increases the simulated ICNC also in Alpine mixed-phase clouds and thereby leads to a better agreement with
observations, while DS did not significantly contribute to the simulated ICNC.

In our study, we use the WRF model including the modified Morrison microphysics scheme from Sotiropoulou et al. (2021) and
Georgakaki et al. (2022) for a case study from a campaign at the Svalbard archipelago where information about the presence
75 of SIP is available from field measurements (Pasquier et al., 2022b). The Ny-Ålesund Aerosol Cloud Experiment (NASCENT)
study took place from September 2019 to August 2020 in Ny-Ålesund, Svalbard (78.9°N, 11.9°E) (Pasquier et al., 2022a).
One of its central objectives was to determine under which conditions either INPs or secondary ice production (SIP) domi-
nantly affect the phase partitioning inside Arctic mixed-phase clouds. For a deeper understanding of this dependency, here we
complement the performed observations with a regional modeling study. We are particularly interested in whether the model
80 can simulate an ICNC as high as observed when using measured INPC and added SIP processes.

A description of the used observations is given in Section 2, while modeling methods follow in Section 3. Section 4 comprises
results and discussion before the conclusions are presented in Section 5.

2 Observations

85 We first present the relevant measurements from the campaign and then describe the meteorological situation of the chosen
case study.

2.1 Instruments and measurements

In this study we utilize the extensive suite of aerosol and cloud measurements conducted during the NASCENT campaign (Pasquier et al., 2022a), which took place over an entire year (fall 2019-2020) in and around the Norwegian research village,

90   Ny-Ålesund (78.9° N, 11.9° E). The measurements we use here are concentrations of aerosols suitable to act as CCN and INPs, measured at the ground, as well as ice crystal and cloud droplet number and mass concentrations, measured in-cloud from the holographic imager HOLIMO onboard the tethered balloon system HoloBalloon (Ramelli et al., 2020).

The CCN concentration (CCNC) was assessed from the concentration of aerosols larger than 70 nm as particles of these sizes can be used as a proxy for CCN (Koike et al., 2019; Pasquier et al., 2022a).

95   To quantify the INP concentrations, aerosols were sampled through an inlet in a container installed at the balloon launch site, using 1) the Horizontal Ice Nucleating Chamber (HINC; Lacher et al. (2017); Mahrt et al. (2018)) and 2) a high-flow rate liquid impinger (Bertin Coriolis-u) with subsequent analysis using the DRoplet Ice Nuclei Counter Zurich (DRINCZ; David et al. (2019a); Wieder et al. (2022b)). Both techniques measure INPs in the immersion mode (Li et al., 2022). It is important to note that due to the efficiency of the liquid-impinger, only aerosols larger than 500 nm could be assessed for their ice nucleating

100   ability in DRINCZ. However, previous studies have shown that aerosols larger than 500 nm make up the largest fraction of the INP population (DeMott et al., 2010; Mason et al., 2015). HoloBalloon itself, or more precisely HOLIMO3B onboard it, provides hydrometeor number and size concentrations measured at altitudes up to 850 m. The technical setup and pixel size restrict the detection of small particles to diameters larger than 6 μm and up to 2 mm (Ramelli et al., 2020). The holographic imager sampled a 15.5 cm^3 volume of cloud at a rate of 6 Hz during the flights (Pasquier et al., 2022a, supplement). For this

105   study, we use the hydrometeor number and size concentrations accumulated over 30 s, 60 s or 300 s, published in Pasquier et al. (2022c). All of the recorded hydrometeors larger than 25 μm were classified as either liquid droplets or ice particles using supervised machine learning (Touloupas et al., 2020). Meanwhile, all particles smaller than 25 μm were automatically classified as liquid droplets. The phase separated number-size distributions were used to calculate the liquid water content (LWC) and ice water content (IWC). For the IWC, the effective mass-dimensional relationship reported in Cotton et al. (2013)

110   was used. The associated uncertainties when using this approach are discussed in Heymsfield et al. (2010).

2.2 Case study

In this study we focus on the 12 November 2019 cloud event from the NASCENT campaign, when there was observational evidence for a large contribution of secondary ice production to the overall ice formation in the cloud (Pasquier et al., 2022a, b). Pasquier et al. (2022a, b) determined this by following the approach presented in Korolev et al. (2020) where the concentration

115   of small pristine ice crystals with diameters <100 μm is used as a measure to identify regions where recent ice formation occurred. If the concentration of the newly formed ice crystals is larger than the INPC, it can be concluded that SIP was occurring. For a more detailed description of the application during the NASCENT campaign see Pasquier et al. (2022b).

On 12 November, a warm front influenced the weather around Ny-Ålesund (Fig. A1). The surface temperature varied between -3 °C and 0 °C, the dominant wind direction was southwesterly and there was a persistent mixed-phase cloud lasting until

around 21 UTC. As the cloud top rose from ca. 1300 m to 2000 m a.s.l. during the day, the cloud top temperature decreased from around -11 to -14 °C. The cloud base varied between 200 m and 600 m a.s.l. and there were several periods of precipitation, resulting in about 2.4 mm of total precipitation (Pasquier et al., 2022a).

HoloBalloon performed three flights during 12 November 2019: 10:00-11:00, 12:15-14:00 and 14:45-17:00 UTC. The HoloBalloon measurement time spent at a certain altitude was not uniformly distributed, rather, the majority of the sampling time was spent close to the maximum altitude of the flight leading to the highest robustness of the measurements inside the main body of the cloud. The estimated CCNC on 12 November of around $9\,\mathrm{cm}^{-3}$ is within a factor of two of the observed cloud droplet number concentration (CDNC) varying between 5 and $15\,\mathrm{cm}^{-3}$, indicating that droplet formation was CCN limited (Motos et al., 2023). Such low concentrations were also commonly observed in earlier studies of CDNC in aerosol-limited regions (e.g. Mauritsen et al., 2011; Moore et al., 2013). The INP measurements made by DRINCZ during the day were fitted and reported as a function of temperature in Eq. 1 (Pasquier et al., 2022a, Fig. 7). The fit is several orders of magnitude lower than other parametrizations commonly used in weather and climate models that are often developed based on mineral dust or measurements from urban mid-latitude areas (e.g. Tobo et al., 2020), but on a similar order of magnitude to the INPC on other days during the NASCENT campaign (Li et al., 2022) as well as results from field campaigns in other Arctic and remote coastal sites (e.g. Hartmann et al., 2020; McCluskey et al., 2018; DeMott et al., 2016; Sze et al., 2023).

$$n_{\mathrm{INP}}(T)[\mathrm{m}^3] = 1000 \cdot \exp(-0.4146 \cdot (T[\mathrm{K}] - 273.15) - 12.4059) \tag{1}$$

The reported CCNC and INP fit are used to replace default values in the model. This permits a correct quantification of heterogeneous cloud particle formation and also ensures that an agreement of the modeled cloud particle concentrations with observations is accomplished through the correct processes. Details about the model setup and implementation of measured aerosol properties follow in the next section.

3 Modeling setup and methods

All of the simulations presented here were conducted with the WRF model. To accommodate for the different microphysics schemes investigated, two model versions were used, namely version 4.2.1 for simulations with the Milbrandt and Yau (MY) microphysics scheme (Milbrandt and Yau, 2005) and version 4.0.1 for simulations with the Morrison (Morr) microphysics scheme (Morrison et al., 2009; Skamarock et al., 2019). The simulations with the Morr scheme were conducted with this version of WRF so that the modified Morr scheme with the secondary ice production processes implemented by Sotiropoulou et al. (2021) and Georgakaki et al. (2022) could be used. We used a nested setup with three domains, where the outermost domain had a resolution of 15 km, the middle domain had 5 km and the inner domain had 1 km resolution. The geographical extent of the domains is shown in Fig. 1, where the innermost domain spans 100 x 100 km. The number of vertical levels between the surface and 50 hPa was set to 172, whereof 93 are below 3 km altitude. This high vertical resolution was chosen
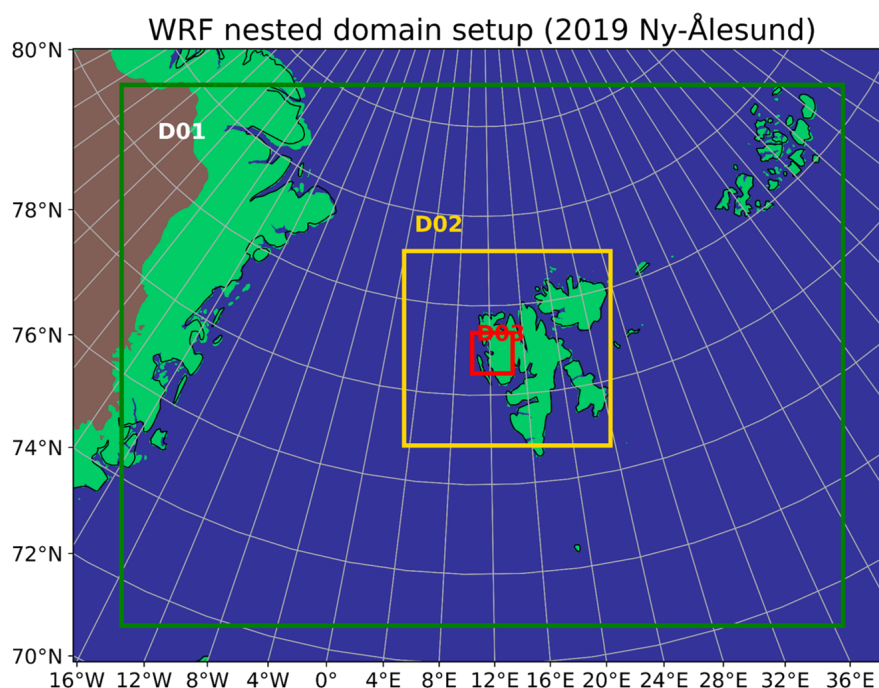
Figure 1. The three nested domains D01, D02 and D03 in the WRF model are shown by the green, yellow and red box, respectively. The associated horizontal resolutions are 15 km, 5 km and 1 km.

to ensure that processes at cloud top and base are resolved in sufficient detail. All of the simulations were initiated on 11 Nov 2019 at 12 UTC, and had a duration of 36 h with a timestep of 30 s. The first 12 h of the simulations were used as spin-up. We initialized and nudged the model using reanalysis data from ERA5 on pressure levels at 00, 06, 12, and 18 UTC on the

155 two outermost domains (Hersbach et al., 2018a, b). Grid nudging was performed for the two horizontal wind components, temperature and specific humidity. No nudging was performed at the surface. As by default in WRF, the nudging strength was $0.0003 \, \text{s}^{-1}$ and nudging lasted for 60 min with a ramp-down at the end of the period. Longwave and shortwave radiation are treated by the CAM scheme (NCAR community atmosphere model, Collins et al. (2004)), and for boundary layer processes we use the YSU scheme (Yonsei University, Hong et al. (2006)). The cumulus parametrization for deep and shallow convection

160 on subgrid scales was only turned on in the largest domain and here we used the scale aware Grell-Freitas ensemble scheme (Grell and Freitas, 2014).

The described settings for domain size, resolution, run duration, time step, nudging, radiation and convection parametrizations are the same for all runs. Changes are only made inside the microphysics schemes and will be explained in the following.

3.1 Microphysics parametrizations

165 To investigate the sensitivity of cloud properties such as CDNC, ICNC, LWC and IWC to both different microphysical parametrizations and to prescribed CCN and INPC, we perform similar sets of simulations with two different microphysics schemes that are described in more detail in the following subsections. Both chosen microphysics schemes are double-moment schemes, but only the MY scheme predicts the CDNC from a prescribed CCNC and ambient supersaturation, while the Morr double-moment scheme uses a prescribed CDNC and therefore is actually only single-moment for cloud droplets. Addition-

170 ally, MY has the largest number of hydrometeor classes, including cloud droplets, cloud ice, rain, snow, graupel and hail while Morr, in its default setup, does not include hail. The reasons for nevertheless focusing most of the study on simulations with the Morr scheme were on one hand that the MY scheme failed to produce a suitable control simulation due to excessive graupel production when CCN/INP concentrations were adapted to observed values (see Section 4.3), and on the other hand and more importantly, because we wanted to apply and test the new SIP implementation recently developed for the Morr scheme by

175 Sotiropoulou et al. (2021) and Georgakaki et al. (2022).

Milbrandt and Yau scheme

In the MY scheme, CCNC and INPC are characterized individually. The default CCNC during negligible vertical motions and downdrafts is $200\,\mathrm{cm^{-3}}$ for continental aerosol and $80\,\mathrm{cm^{-3}}$ when maritime aerosol is selected. By default, continental aerosol is selected and the corresponding value is used across the entire domain. During updrafts, the number of activated CCN

180 is parametrized following Cohard and Pinty (2000), which takes into account local temperature, updraft speed and pressure. The three possible pathways for primary ice production are heterogeneous ice nucleation, homogeneous freezing of cloud droplets, and freezing of rain drops (parametrized after Bigg (1953)). For heterogeneous ice nucleation, a switch enables either 1) the empirical parametrization after Meyers et al. (1992) for deposition and condensation-freezing and contact freezing parametrized following Young (1974) or 2) the parametrization after Cooper (1986) for deposition nucleation and no contact

185 nucleation. As a default, option 1 (Meyers condensation/deposition nucleation and Young contact freezing) is active. Once primary ice is formed, the only SIP process included is RS Hallett and Mossop (1974). Ice mass may also increase from riming. To assess the effect of changing the given aerosol parametrizations towards a more realistic representation of the environmental conditions in our case, we compare two simulations performed with the MY scheme. The first simulation uses the default parametrizations only ($\mathrm{MY_{def}}$). In the second simulation, both the CCNC and INPC are adapted to match the estimated val-

190 ues during 12 November ($\mathrm{MY_{adap}}$) as follows: The CCNC is set to $9\,\mathrm{cm^{-3}}$ during updrafts, negligible vertical motion and downdrafts. Regarding heterogeneous ice nucleation, we chose to stick with the default option (option 1) as it includes contact nucleation, which previous studies have shown is more important in Arctic mixed-phase clouds than deposition freezing (Morrison et al., 2005b, e.g.), and is not active in option 2. We use the contact freezing parametrization by Young (1974), as no measurements of INPs in the contact freezing mode were conducted, but replace the formula for deposition/condensation

195 freezing by Meyers et al. (1992) with the fit for INPC in the immersion mode given in Eq. 1 (Pasquier et al., 2022a). This is because immersion freezing is generally seen as the most common process for ice nucleation in mixed-phase clouds in the

	CCNC [cm^{-3}] when $w \leq 0$	CCNC [cm^{-3}] when $w > 0$	CCN type	deposition/sorption nucleation	contact nucleation	probabilistic rain freezing
MY$_{\text{def}}$	200	Cohard and Pinty (2000)	continental	Meyers et al. (1992)	Young (1974)	Bigg (1953)
MY$_{\text{adap}}$	9	9	maritime	Pasquier et al. (2022a)	Young (1974)	off

Table 1. Overview over simulations for 12 Nov 2019 with the Milbrandt and Yau microphysics (MY) scheme: The default scheme has two parametrizations for CCNC depending on the ambient vertical velocity w.

Arctic and in general in supercooled layers warmer than -27 °C (de Boer et al., 2010; Westbrook and Illingworth, 2011; de Boer et al., 2011). Additionally, we turn off the freezing of rain drops in the model, as this process should only happen either because of an immersed INP or upon collisions with an ice particle (both already accounted for). All important parameter differences
200 between the two simulations are given in Table 1.

Morrison scheme

The Morr scheme is described in Morrison et al. (2009) and builds on an older version published in 2005 (Morrison et al., 2005a). It is a double-moment scheme for the hydrometeor species rain, ice, snow and graupel, but only single-moment for cloud droplets as the CDNC is predefined to a certain number. It also contains a switch to include hail as a separate category
205 but this is not applied in this study.

In order for the Morr scheme to accurately represent the observed cloud properties for the correct physical reasons, several adaptations to the Morr scheme were tested and combined. The entire sequence of adaptations is shown in Fig 2 and Table 3. First, we adjusted the CDNC from the default value of 250 cm^{-3} (Morr$_0$) to 9 cm^{-3} (Morr$_1$), to match the observations within a factor of 2 (5-15 cm^{-3} observed) (Pasquier et al., 2022a). Next, we adjusted primary ice production (Morr$_2$). Regarding
210 processes involving INPs, the scheme contains the following: contact freezing parametrized after Meyers et al. (1992), deposition nucleation after Cooper (1986) and immersion freezing of cloud droplets and rain as parameterized by Bigg (1953). It is important to clarify here that Meyers et al. (1992) presented different parametrizations for deposition/condensation freezing and for contact freezing and the formula used here is not the one mentioned during the description of the MY scheme above for condensation/deposition freezing. As the INP concentration during the NASCENT campaign was measured in the immersion
215 mode, we use Eq. 1 retrieved in Ny-Ålesund (Pasquier et al., 2022a) to replace the formula by Bigg (1953) for the immersion freezing of cloud droplets. Along with this change, we introduce the following condition to limit ice nucleation by INPC: New ice crystals are only nucleated if supercooled cloud droplets are present and the number of INPs at the given temperature exceeds the number of ice particles present. This limitation is necessary to prevent infinite ice nucleation as the scheme is not aerosol aware and INPs nucleated earlier in the cloud are not removed (Kärcher and Marcolli, 2021). Before, i.e. in the
220 default scheme (Morr$_0$), the maximum number of newly formed ice crystals through immersion freezing was only limited by the number of available droplets. However, a limitation based on the number of ice crystals existed for deposition nucleation

in the default scheme. As such, we effectively combine these two limitations (ice crystal and cloud droplet number) now for immersion freezing. Based on the same rationale as for MY, we disable immersion freezing of rain and deposition nucleation, but keep the default formula by Meyers et al. (1992) active for contact nucleation. In summary, Morr_2 and MY_{adap} contain comparable microphysical adjustments.

In Morr_3 we keep all of the previous adjustments from Morr_2 and add the SIP processes BR and DS following the parametrizations by Phillips et al. (2017, 2018) implemented into the Morr scheme for WRF by Sotiropoulou et al. (2021) and Georgakaki et al. (2022). As a result of implementing the BR parametrization following Phillips et al. (2017), the rimed fraction of snow and ice particles has to be prescribed and here we use a rimed fraction of 0.4 in all simulations that include BR (Morr_3, Morr_4 and Morr_5). This corresponds to heavily rimed particles and was found to give reasonable results in Sotiropoulou et al. (2021) even though the value in nature is highly variable. We also note that in the scheme by Georgakaki et al. (2022), DS was also allowed to be triggered by the freezing of rain drops in addition to during freezing induced by ice/snow/graupel-rain collisions (true SIP). Here, as we do not allow for immersion freezing of rain (but only cloud droplets), DS only includes events triggered by collisions.

Motivated by the results from Morr_3, we continued by adjusting the mixing ratio thresholds required for RS to occur (Morr_4) and finally the numbers of splinters created per RS event (Morr_5). We found that RS was not active in Morr_3, because the required mixing ratios for RS were not overcome, and none of the newly implemented SIP mechanisms were triggered in a sufficient amount to increase ICNC either (see Sect. 4.4, Appendix C). However, the required mixing ratios for BR and DS used by Sotiropoulou et al. (2021) and Georgakaki et al. (2022) were actually much lower than the ones given by Morrison et al. (2009) for RS. In that light, we adapted the thresholds for RS to occur. In particular, we lowered the snow and graupel water mixing ratio thresholds to match those required for BR during snow-snow and graupel-graupel collisions (10^{-8} kg/kg) and lowered the cloud liquid and rain water mixing ratios to those required for DS induced by rain-ice crystal collisions (10^{-6} kg/kg). Earlier high-resolution modeling studies over the Southern Ocean and the Antarctic showed an improvement in the representation of low-level mixed-phase clouds in models when removing the RS thresholds in the Morr scheme (Sinclair et al., 2016; Young et al., 2019; Atlas et al., 2020, 2022; Sotiropoulou et al., 2021). Sinclair et al. (2016) and Young et al. (2019) only removed thresholds for liquid mixing ratios, while Atlas et al. (2022) explicitly recommend to completely remove all mass thresholds. The mixing ratio threshold values used in the different studies are given in Table 2.

A further discussion of the changes in RS efficiency follows in Sect. 4.5.

3.2 Model-observation comparison methodology

Before comparing observed and simulated cloud properties, we ensure a satisfying model performance by comparing meteorological variables. For that, ambient and dew point temperature from the three radiosondes launched on 12 November are compared with the simulations at the closest grid point and time step. To then compare the observed and simulated hydrometeor concentrations, we take the model grid point that is closest to the location of HoloBalloon and average the simulated cloud properties over the given flight. To ensure that our results were robust, we also calculated these averages including a few neighboring grid points, but this did not alter the results (not shown). To match the data acquisition from HoloBalloon, we
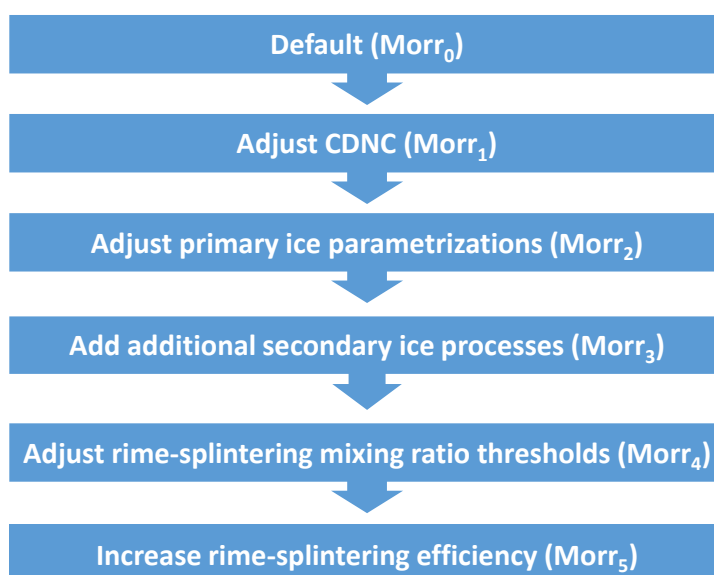
Figure 2. From default to final simulation: The different rows illustrate the steps from the default version of the Morrison scheme towards a version that represents cloud ice correctly. Adjusting CDNC and primary ice parametrizations is done by matching concentrations to observed values of CCNC and INPC. The modifications regarding secondary ice processes are necessary in order to make SIP as efficient in the model as it has been observed in this case.

	Snow - liquid				Graupel - liquid		
	q_{snow}	$q_{cloud\ liquid}$	q_{rain}		$q_{graupel}$	$q_{cloud\ liquid}$	q_{rain}
Default ($Morr_0$-$Morr_3$)	10^{-4}	$0.5 \cdot 10^{-3}$	10^{-4}		10^{-4}	$0.5 \cdot 10^{-3}$	10^{-4}
$Morr_4$, $Morr_5$	10^{-8}	10^{-6}	10^{-6}		10^{-8}	10^{-6}	10^{-6}
Sinclair et al. (2016); Young et al. (2019)	10^{-4}	removed (≈ 0)	removed (≈ 0)		10^{-4}	removed (≈ 0)	removed (≈ 0)
Atlas et al. (2020, 2022)	removed (≈ 0)	removed (≈ 0)	removed (≈ 0)		removed (≈ 0)	removed (≈ 0)	removed (≈ 0)

Table 2. Mixing ratio thresholds in kg/kg that have to be overcome in order for rime splintering to happen in the Morrison microphysics scheme.

	CDNC [cm^{-3}]	contact freezing	heterogeneous nucleation	immersion freezing	rime splintering	add. SIP
$Morr_0$	250	Meyers et al. (1992)	Cooper (1986)	Bigg (1953)	on	no
$Morr_1$	9	Meyers et al. (1992)	Cooper (1986)	Bigg (1953)	on	no
$Morr_2$	9	Meyers et al. (1992)	off	Pasquier et al. (2022a)	on	no
$Morr_3$	9	Meyers et al. (1992)	off	Pasquier et al. (2022a)	on	yes
$Morr_4$	9	Meyers et al. (1992)	off	Pasquier et al. (2022a)	mod.thr.	yes
$Morr_5$	9	Meyers et al. (1992)	off	Pasquier et al. (2022a)	mod. thr., no. splinters*20	yes

Table 3. Overview of runs for 12 Nov 2019 with the Morrison double-moment microphysics scheme (Morr). The parameters changed during different model runs are CDNC, INPC in primary ice production processes, and lower threshold values for mixing ratios during rime splintering. In addition, we implement the secondary ice processes in the Morr microphysics scheme introduced by Sotiropoulou et al. (2021) (BR) and Georgakaki et al. (2022) (DS).

only distinguish between liquid and ice and sum up cloud and rain droplets into one liquid category (Pasquier et al., 2022a). Hence, hereafter the total LWC and CDNC always refer to the combined liquid category. Similarly, all ice particles are merged into one ice category characterized by total IWC and ICNC: these include ice crystals, snow and graupel in the Morr and MY schemes, as well as hail in MY. When comparing LWC, IWC, CDNC and ICNC with the values measured in-situ, we

260   bin the observational data into 100 m intervals between 0 and 800 m altitude, centered around 50 m, 150 m, etc.. The cloud extended to higher altitudes than the tethered balloon was able to reach, therefore a direct comparison is limited to the part of the cloud below 800 m. Finally, we compare the simulated and observed precipitation accumulated over the 24 h of 12 Nov 2019 as well as downward longwave radiation at the surface. Total precipitation was measured using a single-fenced gauge, while the downward longwave radiation measurements were performed and provided by the French-German AWIPEV Re-
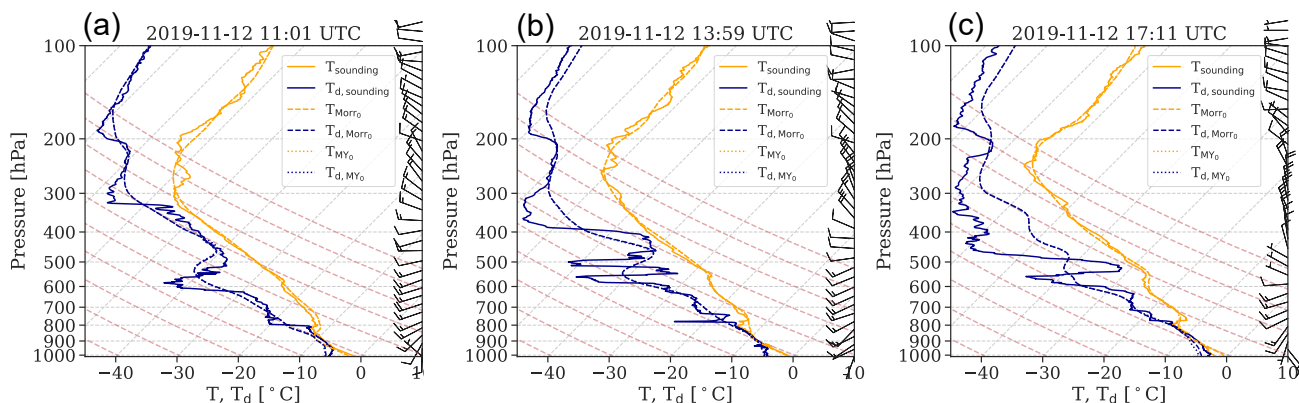
Figure 3. Simulated and radiosonde profiles of temperature (orange) and dew point temperature (blue) over Ny-Ålesund: Here the radiosoundings at (a) 11, (b) 14 and (c) 17 UTC (solid lines) are shown along with the simulations MY_{def} (dotted) and $Morr_0$ (dashed) at the same given times. During the majority of altitudes and times, the profiles for MY_{def} are not distinguishable as its values are identical with $Morr_0$. For illustration of the meteorological situation, we show the wind barbs from the sounding observations in addition.

265 search Base (Maturilli, 2019). As solid and mixed-phase precipitation is known to be underestimated when using single-fenced gauges (Wolff et al., 2015; Kochendorfer et al., 2017; Nitu et al., 2018), we adjust for this under-catch. In a simple estimate, we add 24% to the measured total precipitation which is the average under-catch reported for single-Alter-shielded gauges by Kochendorfer et al. (2017).

4 Results and Discussion

270 Before comparing the influence of the various microphysical parameterization changes in the model, we verify the model performance by comparing the simulated meteorological conditions with radiosonde observations (Fig. 3). The simulated temperature profiles over Ny-Ålesund from the MY_{def} and $Morr_0$ simulations match the 11, 14 and 17 UTC radiosonde temperatures very well (mean deviation of $0.76\,°C$ for both MY and Morr, see Fig. 3). The simulations also capture the dew point temperature profile well (mean deviation of $2.56\,°C$ for MY and $2.55\,°C$ for Morr), especially at lower altitudes up

275 to $750\,hPa$ where the cloud was present during the simulations ($0.97\,°C$ mean deviation for MY, $0.90\,°C$ for Morr). With the simulated meteorological conditions validated when using the two microphysics schemes, we now assess the simulated macrophysical structure of the cloud before comparing the results from the MY and Morrison schemes against each other. Finally, we discuss the impact of the changes within the respective microphysics schemes.

4.1 Cloud macrophysics

280 Before diving into the analysis of microphysical cloud properties, it is reassuring to see that the macroscopic evolution of the cloud on Nov 12 agrees well between simulations and radar observations (see Fig. 4). Throughout the day, the observed
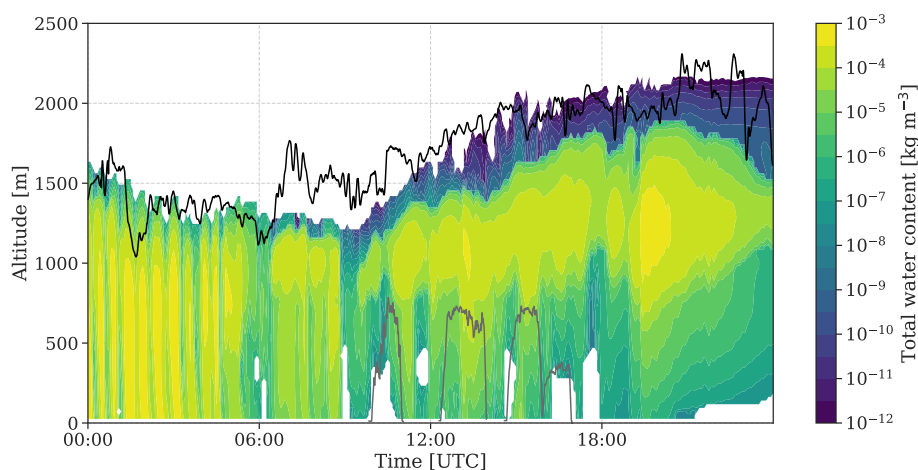
Figure 4. Total water content on 12 November as modeled by the final simulation Morr_5. The macrophysical shape of the cloud agrees well with observations of radar reflectivity (see Pasquier et al. (2022b, Fig. 3c)). The black lines show the observed cloud top as retrieved from radar measurements (Ebell et al., 2022) while the three flights performed by HoloBalloon are shown as grey lines.

and simulated cloud top rises from ca. 1300 m at 6 UTC to around 2000 m at 18 UTC. This is true for simulations with both microphysics schemes and, relative to the increase in cloud top height throughout the day, variations in cloud top height between the different simulations are small (Figs. 5,6). This indicates that the changes in cloud microphysical properties discussed in subsequent sections are primarily caused by differences in the specific microphysics scheme and not by accompanying changes in cloud structure.

The simulated IWC and ICNC extend to higher altitudes than LWC (and CDNC) during all flights, indicating an ice-topped mixed-phase cloud (liquid only below ca. 1300 m vs. ice until 1450 m during the first and ca. 1800 m vs. 2000 m during the third flight, see Figs. 5,6). This result is in agreement with the Cloudnet classification (available from the Cloudnet data portal) that also identifies the cloud as ice-topped (Ebell et al., 2022). Previous observational studies have frequently observed liquid-topped mixed-phase clouds in the Arctic (de Boer et al., 2009; Morrison et al., 2012, e.g.). Therefore, the ice at cloud top in this case study may be a result of local effects (e.g. orography) or the synoptic situation.

4.2 Microphysics scheme intercomparison

In order to assess the influence of the MY and Morr schemes on the simulated cloud microphysics, here we compare the results of the simulations using the two schemes in their default configurations (MY_{def} and Morr_0, as described in Section 3.1). When comparing with the HoloBalloon measurements, it becomes clear that near the maximum flight altitude of HoloBalloon, the LWC is well captured by both simulations (see Fig. 5d and 6c). However, both MY_{def} and Morr_0 are unable to reproduce the LWC below 650 m, except for MY_{def} during flight 1. Simultaneously, MY_{def} and Morr_0 underestimate IWC, particularly during the first flight. While the IWC magnitude is wrong in the simulations, they both have an almost constant value throughout

the atmospheric layer considered, which is consistent with the observations. MY_{def} is in slightly better agreement with the observed ICNC than $Morr_0$ but both simulations maintain too few ice crystals near the surface. This comparison suggests that relative to the observations the ice crystal aggregation may be too efficient in the default schemes, both MY_{def} and $Morr_0$, as evident by the near constant IWC and rapid decrease in ICNC towards the surface relative to the observations (Fig. 5a,b, 6a,b). The influence of constraining these two microphysical parametrizations with aerosol observations and the cause for these systematic biases in the default versions are discussed in the following sections.

4.3 Simulations using the Milbrandt and Yau microphysics scheme

As described in the previous section, MY_{def} struggles to maintain enough LWC and CDNC below $650\,m$ (Fig. 5c,d). The underestimation of liquid at lower altitudes is not overcome when the CCNC is adapted to observed values in MY_{adap}, but the representation is improved slightly, especially during flight 1. Meanwhile, the agreement between observed and simulated LWC is good around $750\,m$ (Fig. 5d). Additionally taking the lowest part of the sounding comparison below $900\,hPa$ into account (Fig. 3), this indicates that, at least during parts of the day, the simulated water vapor pressure is too little just above the surface. Thereby, the lifting condensation level, where dew point and absolute temperature are equal, is located too high in the model, which is visible from the soundings at 11 and 17 UTC (Fig. 3a,c). Nonetheless, at 14 UTC, there is no such discrepancy between simulated and observed dew point at the lowest altitudes (Fig. 3b).

Compared to CDNC and LWC, variations in ICNC and IWC are much larger between the two simulations. In MY_{adap}, the ICNC increases from MY_{def} and even surpasses the observed ICNC (Fig. 5a). This is quite surprising, as the INPC is significantly reduced in MY_{adap} relative to MY_{def}. Upon further investigation, we find that the majority of the ICNC (and IWC) in MY_{adap} is comprised of graupel (see Fig. 7), which is similar to the simulation in Pasquier et al. (2022a), but was not observed. To determine the major cause for this increase in graupel concentrations between MY_{def} and MY_{adap}, we systematically performed simulations with only certain changes included at a time and found that the change in CCNC during updrafts is the determining factor for the increase in graupel number. In a simulation where all adaptions given in Table 1 are included, except the CCNC during updrafts, which is kept parameterized following Cohard and Pinty (2000), the ICNC decreases and is lower than in MY_{def}, consistent with what we expected from lowering INP concentrations. In that case, the ICNC is two to three orders of magnitude lower than observed and not dominated by graupel (Fig. B1). These results show that MY_{def} simulated the observed ICNC reasonably well, but for the wrong reasons, i.e. because of higher CCNC and INPC than observed. Instead, we expect SIP to be the missing process needed to simulate the cloud microphysical properties correctly and for the right reasons. Before an assessment of the effectiveness of SIP follows in the next section using the Morr scheme, we now shortly elaborate on the relevance of looking at the differences between flights as well as at the agreement between simulated and observed precipitation and radiation.

Both the observations and simulations show variations in hydrometeor concentrations between flights, representing different environmental conditions throughout the day. This increases the credibility of the study's results even though the scope is limited to one day. The inter-flight spread in MY_{adap}, however, reveals that this simulation does not capture the change in ICNC, IWC and LWC between flight 1 and the subsequent flights correctly.
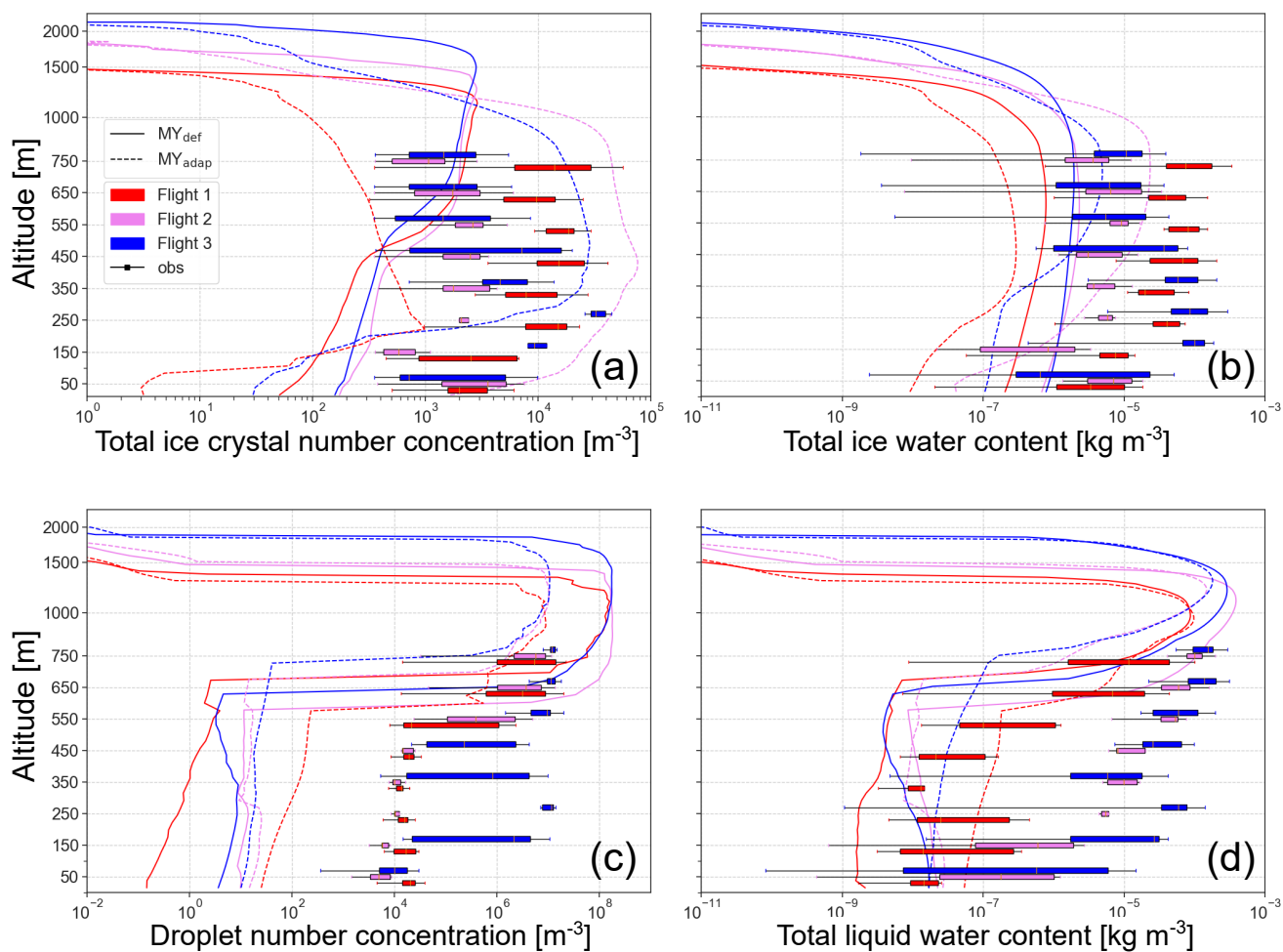
Figure 5. (a) Total ICNC, (b) IWC, (c) CDNC and (d) LWC on 12 Nov 2019 from the two simulations with the MY microphysics scheme. The different colors indicate the different balloon flights: flight 1 (10:00-11:00 UTC) in red, flight 2 (12:15-14:00 UTC) in violet, flight 3 (14:45-17:00 UTC) in blue. The different line styles indicate different simulations (solid line for MY_{def}, dashed line for MY_{adap}). The bar diagrams show observations put together in 100 m-bins between 0 and 800 m altitude, centered around 50 m, 150 m, etc.. Note that the y-axis is linear from the surface up to 800 m and continues logarithmic above to highlight the region where measurements are available.
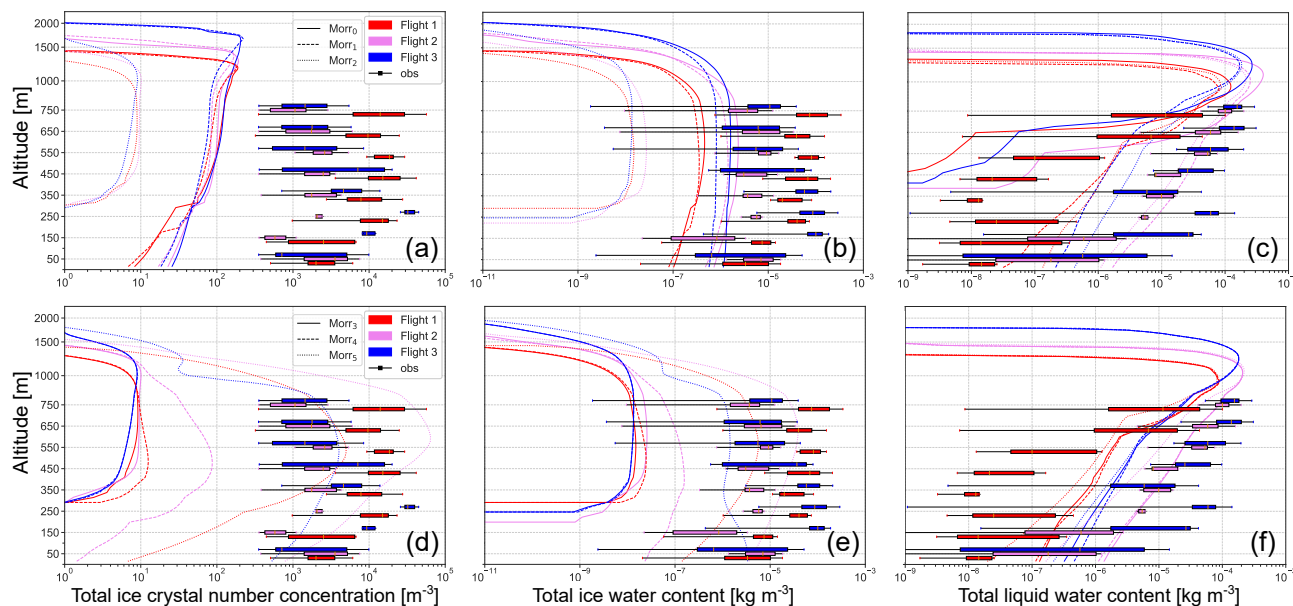
Figure 6. Same as Fig. 5, but for the simulations with the Morrison microphysics scheme and without showing droplet number concentration as this was predefined in the Morr scheme. Panels (a)-(c) show the simulations $Morr_0$-$Morr_2$, while (d)-(f) show the simulations $Morr_3$-$Morr_5$. The three balloon flights are marked by different colors, the simulations are distinguishable by linestyle. The profiles from $Morr_2$ (upper row, dotted line) and $Morr_3$ (lower row, solid line) look identical.

In addition to hydrometeor profiles, we assess precipitation accumulated over 24 h. The lack of simulated CDNC near the
335 surface and the stronger reduction in ICNC and IWC towards the surface than observed lead to a strong underestimation of precipitation in both simulations (Fig. 8).

Downward longwave radiation at the surface is lower than observed in both simulations, but the differences are small compared to the variability during the day. The underestimation of downward longwave radiation can be explained by a stronger simulated reduction in cloud water content towards the surface and thereby on average a higher and colder cloud base.

340 Overall, our results show that the simulations with the MY scheme struggle to represent observed precipitation as well as observed CDNC and LWC at lower altitudes. Even though simulated ICNC and IWC agree better with observations, this is due to a higher CCNC and INPC than observed in MY_{def} and due to a too high simulated graupel production in MY_{adap}, whereas we expect a strong SIP to be the missing element.

4.4 Simulations using the Morrison microphysics scheme

345 In this section, we show the results from six simulations with the Morr scheme, starting with the default version, $Morr_0$. Regarding ICNC, the maximum simulated value in $Morr_0$ is around $200\,m^{-3}$ and thereby, depending on flight number and altitude, at least one order of magnitude below the observations (Fig. 6a). Also, the liquid part of the cloud has a base at ca. 400 m
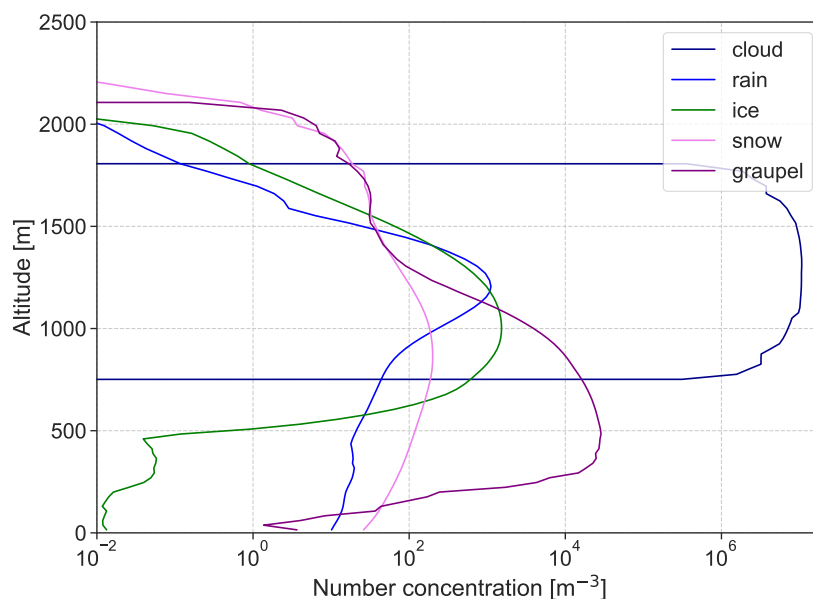
Figure 7. Number concentrations of individual hydrometeor categories in simulation MY_{adap} during the third flight.

in contrast to the observations measuring liquid hydrometeors all the way to the surface (see Fig. 6c). This disagreement in LWC towards the surface is fixed by adapting the CDNC to the observed value of $9\,cm^{-3}$, as done in simulation $Morr_1$, which

350 apart from the updated CDNC, has the same settings as $Morr_0$. The reduced CDNC also results in an increase in the liquid precipitation simulated by $Morr_1$, from 0.12 mm in $Morr_0$ to 0.59 mm during 24 h on 12 Nov (Fig. 8). This can be explained by fewer and larger droplets formed that more rapidly are converted to rain and fall out. However, it is important to note that in both $Morr_0$ and $Morr_1$, the majority of the precipitation is simulated during the early morning hours of Nov 12 and not during daytime when the balloon flights took place (not shown). Meanwhile, as expected, the IWC and ICNC are not impacted and

355 remain on the same order of magnitude as in $Morr_0$. Adapting the CDNC to the observed value results in a slight decrease in snowfall, but not by as much as the rainfall increases, leading to an increase in total precipitation (Fig. 8).

When adapting the primary ice production via the INP concentration fit retrieved from the campaign measurements (as described in Section 3.1) in $Morr_2$, the total ICNC and IWC decrease substantially, as expected. Ice (number and mass) no longer reaches the surface and even above ca. 300 m the ICNC and IWC decrease by approximately one and two orders of magnitude,

360 respectively. As expected, this results in the suppression of the simulated snowfall at the surface, but also in a slight decrease in the total accumulated precipitation to 0.48 mm (Fig. 8).

The decrease in ICNC after adjusting primary ice production should according to expectations be counteracted in $Morr_3$ when more SIP processes are added following Sotiropoulou et al. (2021) and Georgakaki et al. (2022). However, this does not reduce the large discrepancy between the simulated and observed ICNC and the results of $Morr_3$ are in fact very similar to those of

365 Morr$_2$ (Fig. 6a,d). To understand why implementing SIP in the simulation does not lead to a substantial difference between Morr$_2$ and Morr$_3$, we examined the process tendencies from the model output in Morr$_3$ (similar to Fig. 10 where this is shown for Morr$_4$ and Morr$_5$). This allows us to quantify the contribution of the different processes, i.e. primary and secondary ice production processes, to the number of ice crystals formed.

In Morr$_3$ as well as the following simulations, we see that immersion freezing is mainly active at cloud top where the coldest
370 temperatures occur, while contact freezing dominates inside the cloud (shown for Morr$_5$ in Fig. 10a). Meanwhile, in terms of SIP, RS did not occur in Morr$_3$ over Ny-Ålesund, even though a large portion of the cloud was within the RS temperature range and riming was occurring. BR occurred occasionally in Morr$_3$ but produced less ice crystals than primary ice production and DS occurred only sporadically but did not yield a substantial contribution to ice production (not shown).

Even though additional processes were implemented in Morr$_3$, they did not increase the ICNC compared to Morr$_2$ and the
375 simulated ICNC still differed from the observations, as evidence of SIP was observed by HoloBalloon (Pasquier et al., 2022b). To investigate this discrepancy, we first adapted the required mixing ratio thresholds for RS to occur and then increased the number of splinters produced during RS in the following Section (Sect. 4.5).

4.5 Role of secondary ice

380 Contrary to our expectations, activating the SIP processes included in the Morr scheme by Sotiropoulou et al. (2021) did not immediately increase the ICNC. To investigate this surprising finding, we first lowered the thresholds required for RS to occur. Specifically, we set the cloud liquid/rain water and snow/graupel water mixing ratio thresholds to 10^{-8} and 10^{-6} kg/kg, respectively (see Tab. 2). The impact of lowering these thresholds is investigated in Morr$_4$ and results in a flight dependent change in the ICNC. Because graupel concentrations were negligible compared to snow in simulations with the Morr scheme,
385 we focus on splintering events involving snow. Then, for RS to be able to occur in the model at a given time and altitude, the temperature must be within the given range (-8 °C < T < -3 °C), the snow water mixing ratio threshold must be overcome and, in addition, either the cloud liquid or rain water mixing ratio threshold must be overcome. The overview over in which altitude region and during which flight the individual conditions and the joint condition are fulfilled is given in Table C1 and explains the differences in the simulated impact of the RS process during different flights well. We find that the simulated snow water
390 mixing ratio and the temperature are most influential in defining the RS active region, whereas the liquid water mixing ratio thresholds do not substantially limit the region further. As a result, during flight 1 and 2, the simulated ICNC increases by a factor of up to 2 and up to 10, respectively, while during flight 3 hardly any change in ICNC is simulated (see Fig. 6d, simulations Morr$_3$ and Morr$_4$). The latter is because the simulated snow water mixing ratio does not overcome the threshold at any altitude during the third flight. It should be noted that this is in contradiction with the observations, as HOLIMO measured the
395 most SIP during flight 3. Along with RS, BR also became active during flight 1 and 2. Meanwhile, Morr$_4$ only showed a very minor contribution to the increase in ICNC from DS, and only during flight 2 (Fig. 10c). We discuss the relative importance of the different SIP mechanisms after presenting the results of the last adaption made in the scheme regarding the number of splinters produced during RS.
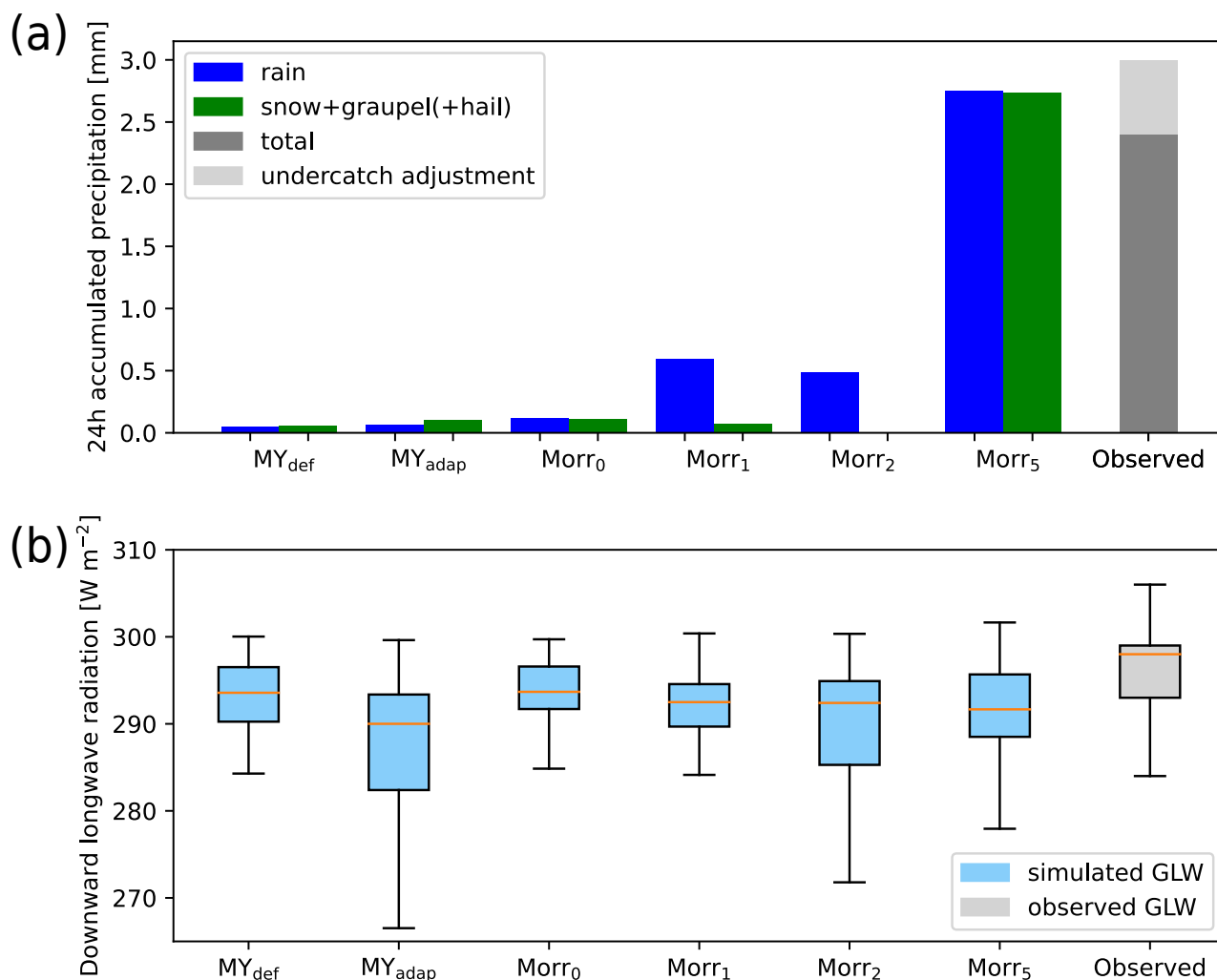
Figure 8. (a) Accumulated precipitation on 12 November, divided in liquid (blue) and frozen fraction (green) and (b) downward longwave radiation at the surface (GLW): Values are shown for the two simulations with the MY scheme, MY_{def} and MY_{adap}, selected simulations with the Morr scheme, and observations (total precipitation shown in grey). As the observed precipitation was measured using a single-fenced gauge, there is likely an under-catch in the amount. Here, we adjust for that by adding 24% following Kochendorfer et al. (2017) (see Sect. 3.2). In the radiation panel (b), the orange lines illustrate the median, the boxes extend from the first to the third quartile of the data and the whisker end points mark the farthest point inside 1.5-times the inter-quartile range from the box. The observed GLW was measured from the French-German AWIPEV Research Base (Maturilli, 2019).

Previous studies have shown that the efficiency of the RS process increases in the presence of large cloud droplets (e.g. Mossop,
400   1978). As relatively large cloud droplets were observed during this case (Pasquier et al., 2022b, a), here we assess the impact
of increasing the number of splinters produced by the RS process by a factor of 20 in the Morr$_5$ simulation (see Sect. 3.1). We
justify this step by considering that cloud droplets in Arctic pristine conditions may be larger and lead to more splinters.

Even though the mixing ratio thresholds are not modified between Morr$_4$ and Morr$_5$, increasing the number of splinters gen-
erated influences the total ICNC during all flights. This increase in ICNC leads to a subsequent increase in BR, which in
405   combination with the initial increase in ICNC from RS leads to a total increase in ICNC by up to three orders of magnitude,
with BR making up a large share of that increase (Fig. 10b). This effectively leads to a "cascading" process of ice production
as observed in field observations (Lawson et al., 2015; Pasquier et al., 2022b).

When comparing between the observed and simulated SIP mechanisms, the observations indicate a more prominent contribu-
tion of SIP from DS (Pasquier et al., 2022a). In contrast, Morr$_5$ simulates that DS is not a determining factor in the increase
410   in ICNC and only active at altitudes below 500 m/near cloud base (Fig. 10b). However, as the in-situ observations were made
near cloud base, the fact that Morr$_5$ also simulates a contribution from DS in this region indicates that even though the model
underestimates the contribution from DS, it is simulating it in the correct place. Additionally, it should be noted that near
cloud base, where DS was observed and simulated, the temperatures were within the RS range. This, in combination with the
observed frozen/fragmented droplets and rimed columns/lollipop ice (Pasquier et al., 2022a), makes it difficult to disentangle
415   the true contributions from RS and DS from the measurements.

Nevertheless, our result that DS had a minor effect on the simulated ICNC is in agreement with the modelling study of
wintertime alpine mixed-phase clouds by Georgakaki et al. (2022), which was conducted with the same modified Morrison
microphysics scheme in WRF. This suggests a bias toward low DS activity in this scheme. As a possible key to alter this bias,
two studies using the Morr microphysics scheme in global models suggest that, if a different size representation, i.e. a bin rep-
420   resentation for the radius instead of a bulk representation of the particle mass, is used for cloud droplets during the treatment
of DS, the magnitude of DS increases (Zhao et al., 2021; Sotiropoulou et al., 2022).

BR played the largest role in increasing ICNC not only in our case, but also in Georgakaki et al. (2022) and Sotiropoulou et al.
(2021). However, Georgakaki et al. (2022) found that in their case falling ice crystals from aloft were important in initiating
BR, which was not the case here. Sotiropoulou et al. (2021) also found that even with RS completely deactivated, BR alone
425   could represent the observed ICNCs in Antarctic summer clouds. At the same time they admit that primary ice production
might have been overestimated in their setup.

In our simulations with constrained CCNC and INPC, and thus a realistic representation of primary ice production, we chose
to reduce the thresholds for RS instead of removing them, as Sotiropoulou et al. (2021) hypothesized that removing all mass
thresholds for RS overestimated RS. As previously stated, when the number of splinters is in addition increased relative to
430   the default parametrization, our simulation results match the observed ICNC very well (Fig. 6d). This result is in accordance
with Young et al. (2019) who also found the best agreement between model and observations when removing the RS liquid
mixing ratio threshold and making RS ten times more efficient in Arctic clouds. This may be due to the high concentration
of large droplets observed in this case and typically found in the Arctic. When comparing the patterns in spatial and temporal

extent of the SIP active regions for BR, RS and DS (Fig. 10b,c), it becomes clear that the higher number of splinters from RS
in $Morr_5$ also strongly affects the activity of BR and DS. For example, during flight 3 where RS was not simulated in $Morr_4$
(Fig. 10c), SIP anyway became active enough to represent the observed ICNC in $Morr_5$ after increasing the number of splinters
produced (Fig. 6f, blue dotted line). Overall, the activity of RS, BR and DS in time changes, e.g. due to the advection of ice
particles between grid boxes, and a higher ICNC is maintained, in turn again favoring more SIP. Finally, our results show that
in situations with constrained CCNC and INPC, maintaining some thresholds for RS works well when the number of splinters
is also increased relative to the default parametrization.

As for the MY simulations, we again assess the accumulated precipitation over 24 h and, here, we find a clear improvement
in the representation in $Morr_5$, especially of solid precipitation (Fig. 8). While highly underestimated in $Morr_0$, now total pre-
cipitation is even overestimated, likely due to a too high amount of supercooled drizzle. Looking at the downward longwave
radiation, the variations in the median are small between the different simulations indicating that the radiative effect of the
cloud is, in contrast to the precipitation, not affected by the introduced changes in microphysical parametrizations. As for MY,
the underestimation of the downward radiation at the surface might come from a slightly higher and colder cloud base.

Overall, $Morr_5$ clearly represents the best match with observations of ICNC and IWC even though the relative importance of
BR and DS does not necessarily reflect the observations. It is the only simulation that produces an as high ICNC as observed
and still represents LWC well and better than the default Morr scheme ($Morr_0$). In addition, it performs best in simulating
enough precipitation. The combination of implemented and enhanced SIP processes is able to reproduce the observed ICNC
and IWC during all flights, although the environmental conditions and the amount of IWC produced through primary ice
production vary. Therefore we consider $Morr_5$ a successful attempt to represent an Arctic mixed-phase cloud with a realistic
distribution of primary and secondary ice production.

5 Conclusions

This study shows that generalized out-of-the-box cloud microphysics schemes, i.e. MY and Morr, can reasonably simulate
the ice and water content of Arctic mixed-phase clouds. However, this reasonable representation occurs for the wrong reasons
due to compensating errors. In the default schemes, the number of available aerosols for nucleating cloud particles is often
unrealistically high for Arctic conditions and the more numerous primary ice production compensates for the lack of secondary
ice production. As shown here, in the pristine Arctic environment of Ny-Ålesund, Svalbard, the low-level mixed-phase cloud
observed on 12 November 2019 is well represented in the WRF model with the default MY and Morr schemes in terms of
macrophysical shape and water content, but the ICNC and the amount of precipitation from the cloud are underestimated. When
the concentrations of aerosols suitable to nucleate cloud particles are adapted to observed values in the MY scheme, the ICNC
increases, but is dominated by graupel which was not observed, but already pointed out in Pasquier et al. (2022a). This increase
in graupel is caused by the lowered CCNC during updrafts, indicating that the MY scheme fails to represent ice production
accurately in environments with very low CCNC. Meanwhile, the underestimation of liquid water towards the surface and of
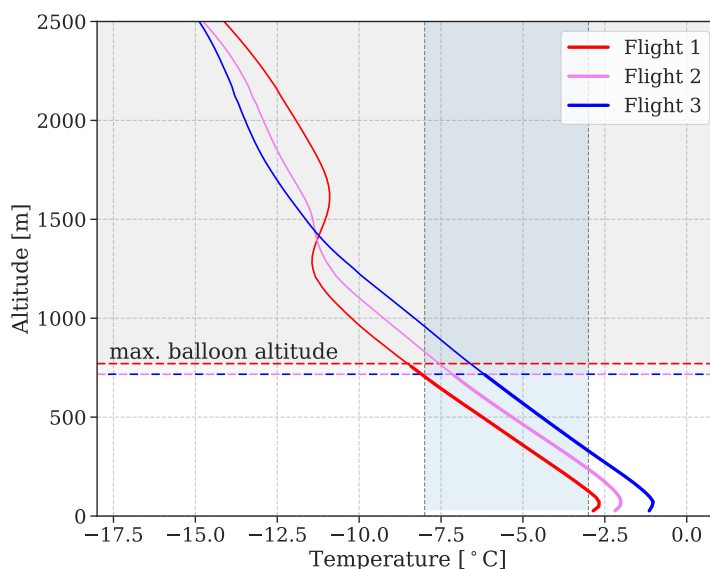
Figure 9. Temperature profiles from the model simulations averaged over the three flight times on 12 November. Here, the profiles from simulation Morr$_4$ are shown, but the choice of simulation does not play a role as the profiles don't vary across simulations. Temperatures below -38 °C, i.e. suitable for homogeneous freezing are reached above ca. 6300 m (not shown). The vertical dashed lines and shading indicate the temperature range where rime splintering is permitted (-8 to -3 °C), the colored horizontal dashed lines indicate the maximum flight altitudes.

precipitation is not altered when aerosol concentrations are changed. In the Morr scheme, however, the simulation matches the observed ICNC and precipitation well, when the concentrations of cloud nucleating aerosols are adapted to observed values, rime splintering is made more efficient and further secondary ice processes are added. The lack of modeled secondary ice
470   production in the default Morr scheme is both due to missing processes (in our case mainly collisional breakup) and too high snow, cloud liquid and rain water mixing ratio thresholds required for rime splintering to occur. Based on the earlier studies by Atlas et al. (2020, 2022); Sotiropoulou et al. (2021, 2020) and the finding in our case that the snow, cloud liquid and rain water mixing ratio never reached the thresholds required for rime splintering to happen in the default scheme, we recommend to lower these mixing ratio thresholds. The fact that the occurrence of rime splintering was needed in order to
475   activate further SIP processes and ultimately represent observed ICNC further supports this recommendation. Otherwise, the thresholds restrict the occurrence of rime splintering to clouds with a higher ice and liquid water content than often observed in the Arctic. Additionally, we increase the number of splinters produced and find that an increase by a factor of 20 yields good agreement with observed ice crystal number concentrations. Based on this and the findings of Young et al. (2019), we hypothesize that this is justified in clean Arctic environments with relatively large droplets, but further laboratory and field
480   studies relating the number of splinters produced by rime splintering to both mixing ratios and droplet sizes are required
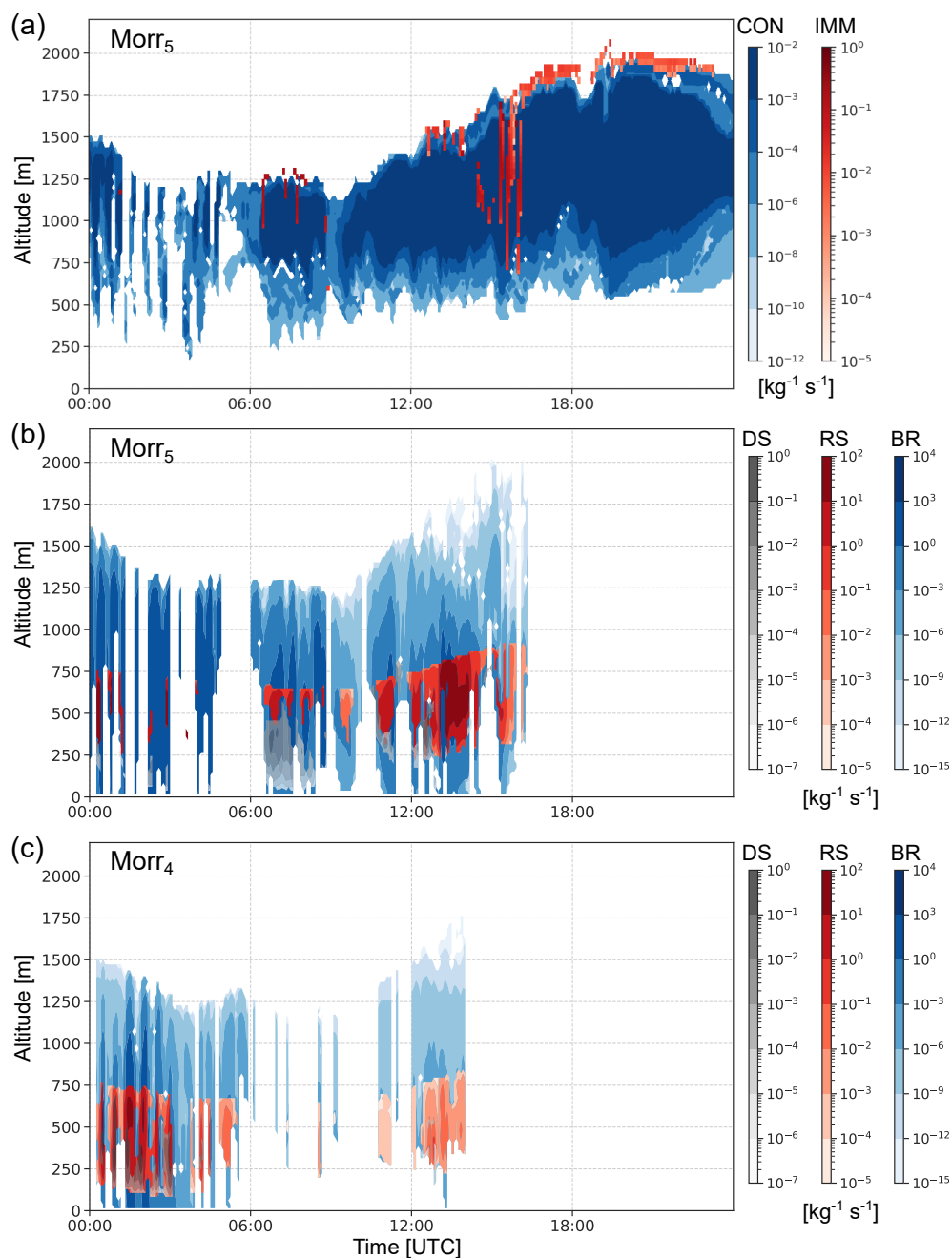
Figure 10. Ice crystal number concentration tendencies of (a) contact (CON, in blue) and immersion freezing (IMM, on top in red) and (b,c) collisional breakup (BR, in blue), rime splintering (RS, on top in red) and droplet shattering (DS, on top in grey): DS is shown partly transparent to visualize that BR is generally active simultaneously. The panels (a) and (b) show simulation $Morr_5$ while the lowermost panel (c) shows the SIP tendencies for simulation $Morr_4$.

to confirm or reject this hypothesis. Apart from ICNC profiles, also the simulated precipitation is considerably improved when aerosols and SIP processes are represented more realistically. Regarding the cloud's radiative effect, the changes in downward longwave radiation changes between default and adapted schemes is small, indicating that the misrepresentation of ice production does not lead to a bias in how much heat is trapped between the cloud and the surface. Even though the changes

485 made between the default simulation $Morr_0$ and the final simulation $Morr_5$ have been validated using the case study on 12 November with observational evidence for strong SIP, the applied modifications are meant to be of a general nature and should not hinder the application to cases where no SIP was observed. Also, the performance across differences in the microphysical conditions between the flights already suggests that the modified scheme is applicable in different conditions. The correct representation of hydrometeor profiles as well as precipitation for the right reason is a prerequisite for model simulations to be

490 used as baselines to investigate cloud responses to aerosol perturbations and future warming.

Code and data availability. The HoloBalloon data is available from Pasquier et al. (2022c). Cloudnet data is provided by the Finnish Meteorological Institute and available under https://cloudnet.fmi.fi. Observations of surface radiation from Ny-Ålesund are available from the World Radiation Monitoring Center - Baseline Surface Radiation Network (https://bsrn.awi.de). The modified Morrison scheme is available on request.

495 **Appendix A: Weather map**

The following figure taken from Pasquier et al. (2022a, Fig. S2) illustrates the meteorological situation around Svalbard in the morning of 12 November 2019.

Appendix B: Impact of adapting updraft CCNC in the MY scheme

As mentioned in Section 4.3, the surprisingly high amount of graupel was not produced when all changes between MY_{def} and

500 MY_{adap} were made except fixing the CCNC during updrafts to the observed value. Instead, the default parametrization by Cohard and Pinty (2000) was used here. The results of this simulation are marked by MY_{CP00} in Fig. B1.

Appendix C: Impact of RS mixing ratio threshold changes on simulated ICNC

Whether the lowering of required mixing ratio thresholds from simulation $Morr_3$ to $Morr_4$ has an effect on the simulated ICNC during one flight, depends on whether the new thresholds were overcome during the time of this flight. To reveal the

505 regions where the lowered mixing ratio thresholds for RS in $Morr_4$ actually enable RS, we show the altitude regions where the individual thresholds are overcome and where the joint condition (see Sect. 4.5) is met in Tab. C1. During flight 1, the flight time-averaged snow mixing ratio in $Morr_4$ just overcame the updated threshold (by less than 50%) at altitudes between 350 and 620 m. At the same time, the temperature criterion was met between 100 and 700 m altitude and the rain mixing ratio exceeded
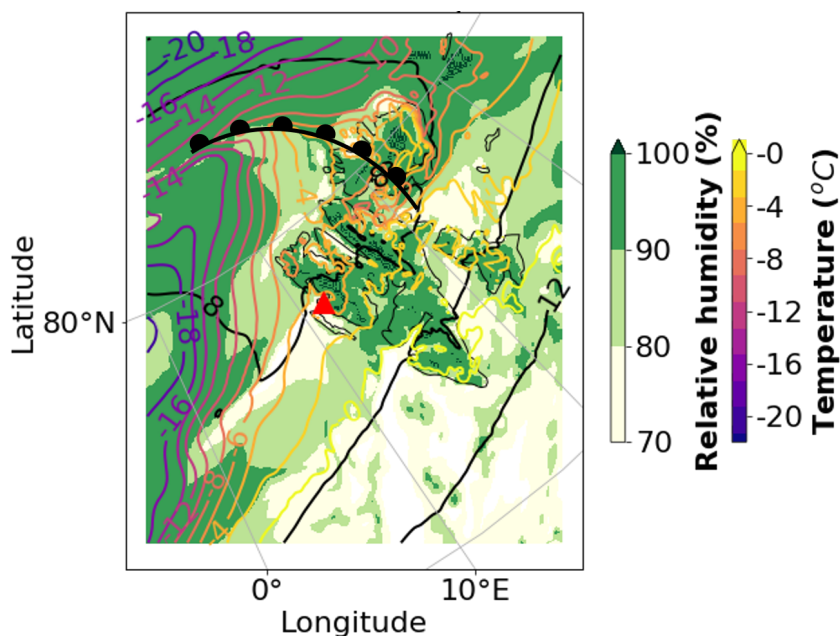
Figure A1. Map showing the synoptic situation with the estimated location of the warm front on 12 November at 06 UTC (figure taken from Pasquier et al. (2022a, Fig. S2), produced using MEPS model data (Hellmuth and Hofer, 2019)): The relative humidity and the temperature at 1000 hPa are indicated by green shading and colored lines, respectively. The red triangle shows the location of Ny-Ålesund.

the threshold above 370 m. Thus, the altitude region where RS involving snow and rain was active during flight 1 is located
510 between 370 and 620 m. RS involving snow and cloud droplets was not occurring during flight 1 as the cloud liquid mixing ratio threshold was not overcome in the altitude region where the amount of snow was sufficiently high. During flight 2, both the snow and rain mixing ratio clearly exceeded the thresholds at all altitudes. Therefore, the impact of lowering the required mixing ratio thresholds is mostly captured during the second flight. The ice part of the cloud now extends to the surface as observed. Similar to during flight 1, the temperature profile leads to RS primarily increasing the ICNC towards cloud base
515 where the cloud is warm enough for RS to be active (Fig. 9). During the third flight, however, the flight-averaged snow water mixing ratio was even lower than in the first flight and did not reach the threshold. This explains the lack of difference in ICNC between $Morr_3$ and $Morr_4$ for the third flight.

Author contributions. BS performed all model simulations, led the analysis and wrote the manuscript. RD and TS contributed to the manuscript and took part in the development of the methods and the discussion of the results. GS and PG provided the code for added
520 SIP in the Morr scheme and assisted in setting it up. JP provided the measurement data and RD also participated in the measurement campaign. PG, JP and GS commented on the final version of the manuscript.
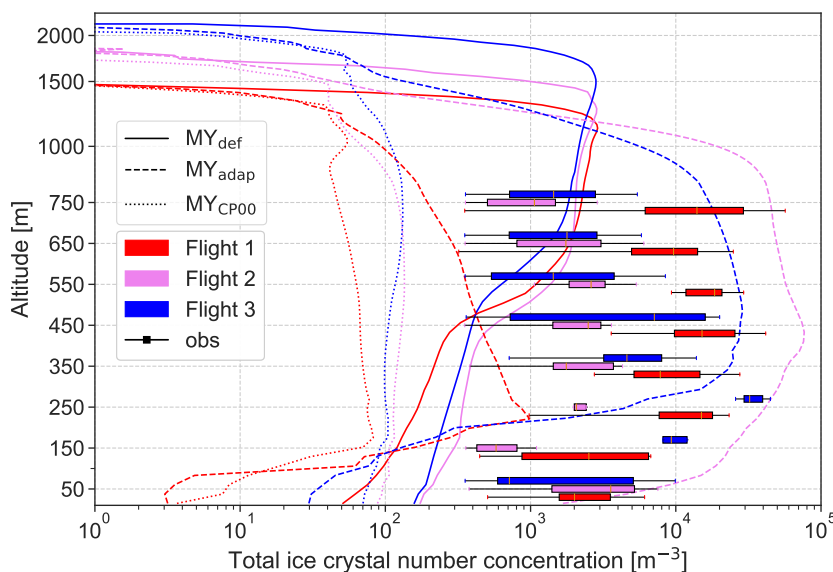
Figure B1. ICNC for the simulations MY_{def}, MY_{adap} and MY_{CP00} which is identical to MY_{adap} apart from the CCNC during updrafts: The ICNC is much lower when CCNC during updrafts is parametrized by Cohard and Pinty (2000) than when it is set to $9\,cm^{-3}$.

	Flight 1	Flight 2	Flight 3
$q_{snow}>10^{-8}$ kg/kg	350-620 m	all altitudes	no altitudes
$q_{cloud\ liquid}>10^{-6}$ kg/kg	above 640 m	above 570 m	above 610 m
$q_{rain}>10^{-6}$ kg/kg	above 370 m	all altitudes	above 200 m
-8 °C < T < -3 °C	100-700 m	250-800 m	350-1000 m
RS active region	370-620 m	250-800 m	no altitudes

Table C1. Regions where criteria for RS are met in Morr$_4$: In order for RS to happen, the threshold for the snow mixing ratio q_{snow} has to be overcome, the temperature must be inside the given range and the cloud water mixing ratio $q_{cloud\ liquid}$ and/or rain water mixing ratio q_{rain} must overcome the threshold. The combination of these limitations results in the RS active region given in the lowest row.

Competing interests. The authors declare that they have no conflict of interests.

Acknowledgements. We gratefully acknowledge the funding by the European Research Council (ERC) through Grant StG758005 and CoG101045273. We would also like to acknowledge EEARO-NO-2019-0423/IceSafari, contract no. 31/2020, under the NO grants 2014–2021
525 of EEA Grants/Norway Grants and funding from the European Union's Horizon research and innovation programme under Grant Agreement 821205 (FORCeS). The simulations were performed on resources provided by Sigma2 - the National Infrastructure for High Performance

Computing and Data Storage in Norway. We would like to thank everyone from ETH Zürich and other institutions who were part of the NASCENT campaign for sharing their dataset. We acknowledge ACTRIS and Finnish Meteorological Institute for providing the cloud classification which is available for download from https://cloudnet.fmi.fi. The cloud radar data for Ny-Ålesund was provided by the University of Cologne, the ceilometer and microwave radiometer data by the Alfred Wegener Institute, Helmholtz Centre for Polar and Marine Research.

References

Atlas, R. L., Bretherton, C. S., Blossey, P. N., Gettelman, A., Bardeen, C., Lin, P., and Ming, Y.: How Well Do Large-Eddy Simulations and Global Climate Models Represent Observed Boundary Layer Structures and Low Clouds Over the Summertime Southern Ocean?, Journal of Advances in Modeling Earth Systems, 12, e2020MS002 205, https://doi.org/https://doi.org/10.1029/2020MS002205, e2020MS002205 10.1029/2020MS002205, 2020.

Atlas, R. L., Bretherton, C. S., Khairoutdinov, M. F., and Blossey, P. N.: Hallett-Mossop Rime Splintering Dims Cumulus Clouds Over the Southern Ocean: New Insight From Nudged Global Storm-Resolving Simulations, AGU Advances, 3, e2021AV000 454, https://doi.org/https://doi.org/10.1029/2021AV000454, e2021AV000454 2021AV000454, 2022.

Auer, A. H., Veal, D. L., and Marwitz, J. D.: Observations of Ice Crystal and Ice Nuclei Concentrations in Stable Cap Clouds, Journal of the Atmospheric Sciences, 26, 1342–1343, 1969.

Barton, N. P., Klein, S. A., Boyle, J. S., and Zhang, Y. Y.: Arctic synoptic regimes: Comparing domain-wide Arctic cloud observations with CAM4 and CAM5 during similar dynamics, Journal of Geophysical Research: Atmospheres, 117, https://doi.org/https://doi.org/10.1029/2012JD017589, 2012.

Beard, K. V.: Ice initiation in warm-base convective clouds: An assessment of microphysical mechanisms, Atmospheric Research, 28, 125–152, https://doi.org/https://doi.org/10.1016/0169-8095(92)90024-5, 1992.

Bigg, E.: The formation of atmospheric ice crystals by the freezing of droplets, Quarterly Journal of the Royal Meteorological Society, 79, 510–519, 1953.

Campbell, J. M. and Christenson, H. K.: Nucleation- and Emergence-Limited Growth of Ice from Pores, Phys. Rev. Lett., 120, 165 701, https://doi.org/10.1103/PhysRevLett.120.165701, 2018.

Cantrell, W. and Heymsfield, A.: Production of Ice in Tropospheric Clouds: A Review, Bulletin of the American Meteorological Society, 86, 795 – 808, https://doi.org/https://doi.org/10.1175/BAMS-86-6-795, 2005.

Carlsen, T. and David, R. O.: Spaceborne Evidence That Ice-Nucleating Particles Influence High-Latitude Cloud Phase, Geophysical Research Letters, 49, e2022GL098 041, https://doi.org/https://doi.org/10.1029/2022GL098041, e2022GL098041 2022GL098041, 2022.

Cohard, J.-M. and Pinty, J.-P.: A comprehensive two-moment warm microphysical bulk scheme. I: Description and tests, Quarterly Journal of the Royal Meteorological Society, 126, 1815–1842, https://doi.org/https://doi.org/10.1002/qj.49712656613, 2000.

Collins, W. D., Rasch, P. J., Boville, B. A., Hack, J. J., McCaa, J. R., Williamson, D. L., Kiehl, J. T., Briegleb, B., Bitz, C., Lin, S.-J., et al.: Description of the NCAR community atmosphere model (CAM 3.0), NCAR Tech. Note NCAR/TN-464+ STR, 226, 2004.

Cooper, W. A.: Ice Initiation in Natural Clouds, pp. 29–32, American Meteorological Society, Boston, MA, https://doi.org/10.1007/978-1-935704-17-1_4, 1986.

Cotton, R. J., Field, P. R., Ulanowski, Z., Kaye, P. H., Hirst, E., Greenaway, R. S., Crawford, I., Crosier, J., and Dorsey, J.: The effective density of small ice particles obtained from in situ aircraft observations of mid-latitude cirrus, Quarterly Journal of the Royal Meteorological Society, 139, 1923–1934, https://doi.org/https://doi.org/10.1002/qj.2058, 2013.

Creamean, J. M., Barry, K., Hill, T. C. J., Hume, C., DeMott, P. J., Shupe, M. D., Dahlke, S., Willmes, S., Schmale, J., Beck, I., Hoppe, C. J. M., Fong, A., Chamberlain, E., Bowman, J., Scharien, R., and Persson, O.: Annual cycle observations of aerosols capable of ice formation in central Arctic clouds, Nature Communications, 13, 3537, https://doi.org/10.1038/s41467-022-31182-x, 2022.

David, R. O., Cascajo-Castresana, M., Brennan, K. P., Rösch, M., Els, N., Werz, J., Weichlinger, V., Boynton, L. S., Bogler, S., Borduas-Dedekind, N., Marcolli, C., and Kanji, Z. A.: Development of the DRoplet Ice Nuclei Counter Zurich (DRINCZ): validation and applica-

tion to field-collected snow samples, Atmospheric Measurement Techniques, 12, 6865–6888, https://doi.org/10.5194/amt-12-6865-2019, 2019a.

570 David, R. O., Marcolli, C., Fahrni, J., Qiu, Y., Sirkin, Y. A. P., Molinero, V., Mahrt, F., Brühwiler, D., Lohmann, U., and Kanji, Z. A.: Pore condensation and freezing is responsible for ice formation below water saturation for porous particles, Proceedings of the National Academy of Sciences, 116, 8184–8189, https://doi.org/10.1073/pnas.1813647116, 2019b.

David, R. O., Fahrni, J., Marcolli, C., Mahrt, F., Brühwiler, D., and Kanji, Z. A.: The role of contact angle and pore width on pore condensation and freezing, Atmospheric Chemistry and Physics, 20, 9419–9440, https://doi.org/10.5194/acp-20-9419-2020, 2020.

575 de Boer, G., Eloranta, E. W., and Shupe, M. D.: Arctic Mixed-Phase Stratiform Cloud Properties from Multiple Years of Surface-Based Measurements at Two High-Latitude Locations, Journal of the Atmospheric Sciences, 66, 2874 – 2887, https://doi.org/https://doi.org/10.1175/2009JAS3029.1, 2009.

de Boer, G., Hashino, T., and Tripoli, G. J.: Ice nucleation through immersion freezing in mixed-phase stratiform clouds: Theory and numer-ical simulations, Atmospheric Research, 96, 315–324, https://doi.org/https://doi.org/10.1016/j.atmosres.2009.09.012, 15th International
580 Conference on Clouds and Precipitation, 2010.

de Boer, G., Morrison, H., Shupe, M. D., and Hildner, R.: Evidence of liquid dependent ice nucleation in high-latitude stratiform clouds from surface remote sensors, Geophysical Research Letters, 38, https://doi.org/https://doi.org/10.1029/2010GL046016, 2011.

DeMott, P. J., Prenni, A. J., Liu, X., Kreidenweis, S. M., Petters, M. D., Twohy, C. H., Richardson, M. S., Eidhammer, T., and Rogers, D. C.: Predicting global atmospheric ice nuclei distributions and their impacts on climate, Proceedings of the National Academy of Sciences,
585 107, 11 217–11 222, https://doi.org/10.1073/pnas.0910818107, 2010.

DeMott, P. J., Hill, T. C. J., McCluskey, C. S., Prather, K. A., Collins, D. B., Sullivan, R. C., Ruppel, M. J., Mason, R. H., Irish, V. E., Lee, T., Hwang, C. Y., Rhee, T. S., Snider, J. R., McMeeking, G. R., Dhaniyala, S., Lewis, E. R., Wentzell, J. J. B., Abbatt, J., Lee, C., Sultana, C. M., Ault, A. P., Axson, J. L., Martinez, M. D., Venero, I., Santos-Figueroa, G., Stokes, M. D., Deane, G. B., Mayol-Bracero, O. L., Grassian, V. H., Bertram, T. H., Bertram, A. K., Moffett, B. F., and Franc, G. D.: Sea spray aerosol as a unique source of ice nucleating
590 particles, Proceedings of the National Academy of Sciences, 113, 5797–5803, https://doi.org/10.1073/pnas.1514034112, 2016.

Diehl, K., Matthias-Maser, S., Jaenicke, R., and Mitra, S.: The ice nucleating ability of pollen:: Part II. Laboratory studies in immersion and contact freezing modes, Atmospheric Research, 61, 125–133, https://doi.org/https://doi.org/10.1016/S0169-8095(01)00132-6, 2002.

Ebell, K., Maturilli, M., and O'Connor, E.: Classification data from Ny-Ålesund on 12 November 2019, https://hdl.handle.net/21.12132/1.9f70b333642f41ab, 2022.

595 Field, P. R., Lawson, R. P., Brown, P. R. A., Lloyd, G., Westbrook, C., Moisseev, D., Miltenberger, A., Nenes, A., Blyth, A., Choular-ton, T., Connolly, P., Buehl, J., Crosier, J., Cui, Z., Dearden, C., DeMott, P., Flossmann, A., Heymsfield, A., Huang, Y., Kalesse, H., Kanji, Z. A., Korolev, A., Kirchgaessner, A., Lasher-Trapp, S., Leisner, T., McFarquhar, G., Phillips, V., Stith, J., and Sullivan, S.: Sec-ondary Ice Production: Current State of the Science and Recommendations for the Future, Meteorological Monographs, 58, 7.1 – 7.20, https://doi.org/https://doi.org/10.1175/AMSMONOGRAPHS-D-16-0014.1, 2017.

600 Fu, S., Deng, X., Shupe, M. D., and Xue, H.: A modelling study of the continuous ice formation in an autumnal Arctic mixed-phase cloud case, Atmospheric Research, 228, 77–85, https://doi.org/https://doi.org/10.1016/j.atmosres.2019.05.021, 2019.

Georgakaki, P., Sotiropoulou, G., Vignon, E., Billault-Roux, A.-C., Berne, A., and Nenes, A.: Secondary ice production processes in winter-time alpine mixed-phase clouds, Atmospheric Chemistry and Physics, 22, 1965–1988, https://doi.org/10.5194/acp-22-1965-2022, 2022.

Gierens, R., Kneifel, S., Shupe, M. D., Ebell, K., Maturilli, M., and Löhnert, U.: Low-level mixed-phase clouds in a complex Arctic environ-
605 ment, Atmospheric Chemistry and Physics, 20, 3459–3481, https://doi.org/10.5194/acp-20-3459-2020, 2020.

Grell, G. A. and Freitas, S. R.: A scale and aerosol aware stochastic convective parameterization for weather and air quality modeling, Atmospheric Chemistry and Physics, 14, 5233–5250, 2014.

Hallett, J. and Mossop, S.: Production of secondary ice particles during the riming process, Nature, 249, 26–28, 1974.

Hartmann, M., Adachi, K., Eppers, O., Haas, C., Herber, A., Holzinger, R., Hünerbein, A., Jäkel, E., Jentzsch, C., van Pinx-
610   teren, M., Wex, H., Willmes, S., and Stratmann, F.: Wintertime Airborne Measurements of Ice Nucleating Particles in the High Arctic: A Hint to a Marine, Biogenic Source for Ice Nucleating Particles, Geophysical Research Letters, 47, e2020GL087 770, https://doi.org/https://doi.org/10.1029/2020GL087770, e2020GL087770 10.1029/2020GL087770, 2020.

Hellmuth, F. and Hofer, S.: Weathermaps from MEPS latest runs, https://github.com/franzihe/Weathermap, 2019.

Hersbach, H., Bell, B., Berrisford, P., Biavati, G., Horányi, A., Muñoz Sabater, J., Nicolas, J., Peubey, C., Radu, R., Rozum, I., Schepers,
615   D., Simmons, A., Soci, C., Dee, D., and Thépaut, J.-N.: ERA5 hourly data on pressure levels from 1979 to present, Copernicus Climate Change Service (C3S) Climate Data Store (CDS) (Accessed on 19-MAR-2021), https://doi.org/10.24381/cds.bd0915c6, 2018a.

Hersbach, H., Bell, B., Berrisford, P., Biavati, G., Horányi, A., Muñoz Sabater, J., Nicolas, J., Peubey, C., Radu, R., Rozum, I., Schepers, D., Simmons, A., Soci, C., Dee, D., and Thépaut, J.-N.: ERA5 hourly data on single levels from 1979 to present, Copernicus Climate Change Service (C3S) Climate Data Store (CDS). (Accessed on 21-APR-2021), https://doi.org/10.24381/cds.adbb2d47, 2018b.

620   Heymsfield, A. J., Schmitt, C., Bansemer, A., and Twohy, C. H.: Improved Representation of Ice Particle Masses Based on Observations in Natural Clouds, Journal of the Atmospheric Sciences, 67, 3303 – 3318, https://doi.org/https://doi.org/10.1175/2010JAS3507.1, 2010.

Hong, S.-Y., Noh, Y., and Dudhia, J.: A new vertical diffusion package with an explicit treatment of entrainment processes, Monthly weather review, 134, 2318–2341, 2006.

Jackson, R. C., McFarquhar, G. M., Korolev, A. V., Earle, M. E., Liu, P. S. K., Lawson, R. P., Brooks, S., Wolde, M., Laskin, A., and Freer, M.:
625   The dependence of ice microphysics on aerosol concentration in arctic mixed-phase stratus clouds during ISDAC and M-PACE, Journal of Geophysical Research: Atmospheres, 117, https://doi.org/https://doi.org/10.1029/2012JD017668, 2012.

Kanji, Z. A., Ladino, L. A., Wex, H., Boose, Y., Burkert-Kohn, M., Cziczo, D. J., and Krämer, M.: Overview of Ice Nucleating Particles, Meteorological Monographs, 58, 1.1 – 1.33, https://doi.org/https://doi.org/10.1175/AMSMONOGRAPHS-D-16-0006.1, 2017.

Karalis, M., Sotiropoulou, G., Abel, S. J., Bossioli, E., Georgakaki, P., Methymaki, G., Nenes, A., and Tombrou, M.: Effects of secondary
630   ice processes on a stratocumulus to cumulus transition during a cold-air outbreak, Atmospheric Research, 277, 106 302, 2022.

Kärcher, B. and Marcolli, C.: Aerosol–cloud interactions: the representation of heterogeneous ice activation in cloud models, Atmospheric Chemistry and Physics, 21, 15 213–15 220, https://doi.org/10.5194/acp-21-15213-2021, 2021.

Keinert, A., Spannagel, D., Leisner, T., and Kiselev, A.: Secondary Ice Production upon Freezing of Freely Falling Drizzle Droplets, Journal of the Atmospheric Sciences, 77, 2959 – 2967, https://doi.org/https://doi.org/10.1175/JAS-D-20-0081.1, 2020.

635   Kochendorfer, J., Nitu, R., Wolff, M., Mekis, E., Rasmussen, R., Baker, B., Earle, M. E., Reverdin, A., Wong, K., Smith, C. D., Yang, D., Roulet, Y.-A., Buisan, S., Laine, T., Lee, G., Aceituno, J. L. C., Alastrué, J., Isaksen, K., Meyers, T., Brækkan, R., Landolt, S., Jachcik, A., and Poikonen, A.: Analysis of single-Alter-shielded and unshielded measurements of mixed and solid precipitation from WMO-SPICE, Hydrology and Earth System Sciences, 21, 3525–3542, https://doi.org/10.5194/hess-21-3525-2017, 2017.

Koike, M., Ukita, J., Ström, J., Tunved, P., Shiobara, M., Vitale, V., Lupi, A., Baumgardner, D., Ritter, C., Hermansen, O., Yamada, K., and
640   Pedersen, C. A.: Year-Round In Situ Measurements of Arctic Low-Level Clouds: Microphysical Properties and Their Relationships With Aerosols, Journal of Geophysical Research: Atmospheres, 124, 1798–1822, https://doi.org/https://doi.org/10.1029/2018JD029802, 2019.

Korolev, A. and Leisner, T.: Review of experimental studies of secondary ice production, Atmospheric Chemistry and Physics, 20, 11 767–11 797, https://doi.org/10.5194/acp-20-11767-2020, 2020.

Korolev, A., Heckman, I., Wolde, M., Ackerman, A. S., Fridlind, A. M., Ladino, L. A., Lawson, R. P., Milbrandt, J., and Williams, E.: A
645   new look at the environmental conditions favorable to secondary ice production, Atmospheric Chemistry and Physics, 20, 1391–1429,
       https://doi.org/10.5194/acp-20-1391-2020, 2020.

Lacher, L., Lohmann, U., Boose, Y., Zipori, A., Herrmann, E., Bukowiecki, N., Steinbacher, M., and Kanji, Z. A.: The Horizontal Ice
       Nucleation Chamber (HINC): INP measurements at conditions relevant for mixed-phase clouds at the High Altitude Research Station
       Jungfraujoch, Atmospheric Chemistry and Physics, 17, 15 199–15 224, https://doi.org/10.5194/acp-17-15199-2017, 2017.

650   Lauber, A., Kiselev, A., Pander, T., Handmann, P., and Leisner, T.: Secondary Ice Formation during Freezing of Levitated Droplets, Journal
       of the Atmospheric Sciences, 75, 2815 – 2826, https://doi.org/https://doi.org/10.1175/JAS-D-18-0052.1, 2018.

Lauber, A., Henneberger, J., Mignani, C., Ramelli, F., Pasquier, J. T., Wieder, J., Hervo, M., and Lohmann, U.: Continuous secondary-ice
       production initiated by updrafts through the melting layer in mountainous regions, Atmospheric Chemistry and Physics, 21, 3855–3870,
       https://doi.org/10.5194/acp-21-3855-2021, 2021.

655   Lawson, R. P., Woods, S., and Morrison, H.: The Microphysics of Ice and Precipitation Development in Tropical Cumulus Clouds, Journal
       of the Atmospheric Sciences, 72, 2429 – 2445, https://doi.org/https://doi.org/10.1175/JAS-D-14-0274.1, 2015.

Li, G., Wieder, J., Pasquier, J. T., Henneberger, J., and Kanji, Z. A.: Predicting atmospheric background number concentration of ice-
       nucleating particles in the Arctic, Atmospheric Chemistry and Physics, 22, 14 441–14 454, https://doi.org/10.5194/acp-22-14441-2022,
       2022.

660   Luo, Y., Xu, K.-M., Morrison, H., and McFarquhar, G.: Arctic Mixed-Phase Clouds Simulated by a Cloud-Resolving Model: Comparison
       with ARM Observations and Sensitivity to Microphysics Parameterizations, Journal of the Atmospheric Sciences, 65, 1285 – 1303,
       https://doi.org/https://doi.org/10.1175/2007JAS2467.1, 2008.

Mahrt, F., Marcolli, C., David, R. O., Grönquist, P., Barthazy Meier, E. J., Lohmann, U., and Kanji, Z. A.: Ice nucleation abilities
       of soot particles determined with the Horizontal Ice Nucleation Chamber, Atmospheric Chemistry and Physics, 18, 13 363–13 392,
665   https://doi.org/10.5194/acp-18-13363-2018, 2018.

Marcolli, C.: Deposition nucleation viewed as homogeneous or immersion freezing in pores and cavities, Atmospheric Chemistry and
       Physics, 14, 2071–2104, https://doi.org/10.5194/acp-14-2071-2014, 2014.

Mason, R. H., Si, M., Li, J., Chou, C., Dickie, R., Toom-Sauntry, D., Pöhlker, C., Yakobi-Hancock, J. D., Ladino, L. A., Jones, K.,
       Leaitch, W. R., Schiller, C. L., Abbatt, J. P. D., Huffman, J. A., and Bertram, A. K.: Ice nucleating particles at a coastal marine bound-
670   ary layer site: correlations with aerosol type and meteorological conditions, Atmospheric Chemistry and Physics, 15, 12 547–12 566,
       https://doi.org/10.5194/acp-15-12547-2015, 2015.

Maturilli,   M.:   Basic   and   other   measurements   of   radiation   at   station   Ny-Ålesund   (2019-11),   PANGAEA,
       https://doi.org/10.1594/PANGAEA.909940, in: Maturilli, M (2020): Basic and other measurements of radiation at station Ny-
       Ålesund (2006-05 et seq). Alfred Wegener Institute - Research Unit Potsdam, PANGAEA, https://doi.org/10.1594/PANGAEA.914927,
675   2019.

Mauritsen, T., Sedlar, J., Tjernström, M., Leck, C., Martin, M., Shupe, M., Sjogren, S., Sierau, B., Persson, P. O. G., Brooks, I. M., and Swi-
       etlicki, E.: An Arctic CCN-limited cloud-aerosol regime, Atmospheric Chemistry and Physics, 11, 165–173, https://doi.org/10.5194/acp-
       11-165-2011, 2011.

McCluskey, C. S., Ovadnevaite, J., Rinaldi, M., Atkinson, J., Belosi, F., Ceburnis, D., Marullo, S., Hill, T. C. J., Lohmann, U., Kanji,
680   Z. A., O'Dowd, C., Kreidenweis, S. M., and DeMott, P. J.: Marine and Terrestrial Organic Ice-Nucleating Particles in Pristine Ma-

rine to Continentally Influenced Northeast Atlantic Air Masses, Journal of Geophysical Research: Atmospheres, 123, 6196–6212, https://doi.org/https://doi.org/10.1029/2017JD028033, 2018.

Meyers, M. P., DeMott, P. J., and Cotton, W. R.: New primary ice-nucleation parameterizations in an explicit cloud model, Journal of Applied Meteorology and Climatology, 31, 708–721, 1992.

685 Milbrandt, J. and Yau, M.: A multimoment bulk microphysics parameterization. Part II: A proposed three-moment closure and scheme description, Journal of Atmospheric Sciences, 62, 3065–3081, https://doi.org/10.1175/JAS3535.1, 2005.

Moore, R. H., Karydis, V. A., Capps, S. L., Lathem, T. L., and Nenes, A.: Droplet number uncertainties associated with CCN: an assessment using observations and a global model adjoint, Atmospheric Chemistry and Physics, 13, 4235–4251, https://doi.org/10.5194/acp-13-4235-2013, 2013.

690 Morrison, H., Curry, J., and Khvorostyanov, V.: A new double-moment microphysics parameterization for application in cloud and climate models. Part I: Description, Journal of the atmospheric sciences, 62, 1665–1677, 2005a.

Morrison, H., Shupe, M. D., Pinto, J. O., and Curry, J. A.: Possible roles of ice nucleation mode and ice nuclei depletion in the extended lifetime of Arctic mixed-phase clouds, Geophysical Research Letters, 32, https://doi.org/https://doi.org/10.1029/2005GL023614, 2005b.

Morrison, H., Thompson, G., and Tatarskii, V.: Impact of cloud microphysics on the development of trailing stratiform precipitation in a
695 simulated squall line: Comparison of one-and two-moment schemes, Monthly weather review, 137, 991–1007, 2009.

Morrison, H., De Boer, G., Feingold, G., Harrington, J., Shupe, M. D., and Sulia, K.: Resilience of persistent Arctic mixed-phase clouds, Nature Geoscience, 5, 11–17, 2012.

Mossop, S. C.: The influence of drop size distribution on the production of secondary ice particles during graupel growth, Quarterly Journal of the Royal Meteorological Society, 104, 323–330, https://doi.org/https://doi.org/10.1002/qj.49710444007, 1978.

700 Motos, G., Freitas, G., Georgakaki, P., Wieder, J., Li, G., Aas, W., Lunder, C., Krejci, R., Pasquier, J. T., Henneberger, J., David, R. O., Ritter, C., Mohr, C., Zieger, P., and Nenes, A.: Aerosol and dynamical contributions to cloud droplet formation in Arctic low-level clouds, EGUsphere, 2023, 1–25, https://doi.org/10.5194/egusphere-2023-530, 2023.

Nitu, R., Roulet, Y.-A., Wolff, M., Earle, M., Reverdin, A., Smith, C., Kochendorfer, J., Morin, S., Rasmussen, R., Wong, K., Alastrué, J., Arnold, L., Baker, B., Buisán, S., Collado, J., Colli, M., Collins, B., Gaydos, A., Hannula, H.-R., Hoover, J., Joe, P., Kontu, A., Laine,
705 T., Lanza, L., Lanzinger, E., Lee, G., Lejeune, Y., Leppänen, L., Mekis, E., Panel, J.-M., Poikonen, A., Ryu, S., Sabatini, F., Theriault, J., Yang, D., Genthon, C., van den Heuvel, F., Hirasawa, N., Konishi, H., Motoyoshi, H., Nakai, S., Nishimura, K., Senese, A., and Yamashita, K.: WMO Solid Precipitation Intercomparison Experiment (SPICE) (2012 - 2015), Tech. Rep. Instruments and Observing Methods (IOM) Report No. 131, World Meteorological Organization, Geneva, Switzerland, https://library.wmo.int/idurl/4/56317, 2018.

Norgren, M. S., de Boer, G., and Shupe, M. D.: Observed aerosol suppression of cloud ice in low-level Arctic mixed-phase clouds, Atmo-
710 spheric Chemistry and Physics, 18, 13 345–13 361, https://doi.org/10.5194/acp-18-13345-2018, 2018.

Pasquier, J. T., David, R. O., Freitas, G., Gierens, R., Gramlich, Y., Haslett, S., Li, G., Schäfer, B., Siegel, K., Wieder, J., Adachi, K., Belosi, F., Carlsen, T., Decesari, S., Ebell, K., Gilardoni, S., Gysel-Beer, M., Henneberger, J., Inoue, J., Kanji, Z. A., Koike, M., Kondo, Y., Krejci, R., Lohmann, U., Maturilli, M., Mazzolla, M., Modini, R., Mohr, C., Motos, G., Nenes, A., Nicosia, A., Ohata, S., Paglione, M., Park, S., Pileci, R. E., Ramelli, F., Rinaldi, M., Ritter, C., Sato, K., Storelvmo, T., Tobo, Y., Traversi, R., Viola, A., and Zieger, P.: The Ny-Ålesund
715 Aerosol Cloud Experiment (NASCENT): Overview and First Results, Bulletin of the American Meteorological Society, 103, E2533 – E2558, https://doi.org/https://doi.org/10.1175/BAMS-D-21-0034.1, 2022a.

Sotiropoulou, G., Sullivan, S., Savre, J., Lloyd, G., Lachlan-Cope, T., Ekman, A. M. L., and Nenes, A.: The impact of secondary ice produc-
tion on Arctic stratocumulus, Atmospheric Chemistry and Physics, 20, 1301–1316, https://doi.org/10.5194/acp-20-1301-2020, 2020.

Sotiropoulou, G., Vignon, E., Young, G., Morrison, H., O'Shea, S. J., Lachlan-Cope, T., Berne, A., and Nenes, A.: Secondary ice production
in summer clouds over the Antarctic coast: an underappreciated process in atmospheric models, Atmospheric Chemistry and Physics, 21,
755–771, https://doi.org/10.5194/acp-21-755-2021, 2021.

Sotiropoulou, G., Lewinschal, A., Georgakaki, P., Phillips, V., Patade, S., Ekman, A. M. L., and Nenes, A.: Sensitivity of Arctic clouds to ice
microphysical processes in the NorESM2 climate model, https://doi.org/10.1002/essoar.10512081.1, 2022.

Sze, K. C. H., Wex, H., Hartmann, M., Skov, H., Massling, A., Villanueva, D., and Stratmann, F.: Ice-nucleating particles in north-
ern Greenland: annual cycles, biological contribution and parameterizations, Atmospheric Chemistry and Physics, 23, 4741–4761,
https://doi.org/10.5194/acp-23-4741-2023, 2023.

Tobo, Y., Uetake, J., Matsui, H., Moteki, N., Uji, Y., Iwamoto, Y., Miura, K., and Misumi, R.: Seasonal Trends of At-
mospheric Ice Nucleating Particles Over Tokyo, Journal of Geophysical Research: Atmospheres, 125, e2020JD033 658,
https://doi.org/https://doi.org/10.1029/2020JD033658, e2020JD033658 2020JD033658-T, 2020.

Touloupas, G., Lauber, A., Henneberger, J., Beck, A., and Lucchi, A.: A convolutional neural network for classifying cloud particles recorded
by imaging probes, Atmospheric Measurement Techniques, 13, 2219–2239, https://doi.org/10.5194/amt-13-2219-2020, 2020.

Vali, G., DeMott, P. J., Möhler, O., and Whale, T. F.: Technical Note: A proposal for ice nucleation terminology, Atmospheric Chemistry and
Physics, 15, 10 263–10 270, https://doi.org/10.5194/acp-15-10263-2015, 2015.

Verlinde, J., Harrington, J. Y., McFarquhar, G. M., Yannuzzi, V. T., Avramov, A., Greenberg, S., Johnson, N., Zhang, G., Poellot, M. R.,
Mather, J. H., Turner, D. D., Eloranta, E. W., Zak, B. D., Prenni, A. J., Daniel, J. S., Kok, G. L., Tobin, D. C., Holz, R., Sassen, K.,
Spangenberg, D., Minnis, P., Tooman, T. P., Ivey, M. D., Richardson, S. J., Bahrmann, C. P., Shupe, M., DeMott, P. J., Heymsfield,
A. J., and Schofield, R.: The Mixed-Phase Arctic Cloud Experiment, Bulletin of the American Meteorological Society, 88, 205 – 222,
https://doi.org/https://doi.org/10.1175/BAMS-88-2-205, 2007.

Wendisch, M., Brückner, M., Burrows, J., Crewell, S., Dethloff, K., Ebell, K., Lüpkes, C., Macke, A., Notholt, J., Quaas, J., et al.: Under-
standing causes and effects of rapid warming in the Arctic, Eos, 98, https://doi.org/10.1029/2017EO064803, 2017.

Wendisch, M., Macke, A., Ehrlich, A., Lüpkes, C., Mech, M., Chechin, D., Dethloff, K., Velasco, C. B., Bozem, H., Brückner, M., Clemen,
H.-C., Crewell, S., Donth, T., Dupuy, R., Ebell, K., Egerer, U., Engelmann, R., Engler, C., Eppers, O., Gehrmann, M., Gong, X.,
Gottschalk, M., Gourbeyre, C., Griesche, H., Hartmann, J., Hartmann, M., Heinold, B., Herber, A., Herrmann, H., Heygster, G., Hoor, P.,
Jafariserajehlou, S., Jäkel, E., Järvinen, E., Jourdan, O., Kästner, U., Kecorius, S., Knudsen, E. M., Köllner, F., Kretzschmar, J., Lelli, L.,
Leroy, D., Maturilli, M., Mei, L., Mertes, S., Mioche, G., Neuber, R., Nicolaus, M., Nomokonova, T., Notholt, J., Palm, M., van Pinx-
teren, M., Quaas, J., Richter, P., Ruiz-Donoso, E., Schäfer, M., Schmieder, K., Schnaiter, M., Schneider, J., Schwarzenböck, A., Seifert, P.,
Shupe, M. D., Siebert, H., Spreen, G., Stapf, J., Stratmann, F., Vogl, T., Welti, A., Wex, H., Wiedensohler, A., Zanatta, M., and Zeppenfeld,
S.: The Arctic Cloud Puzzle: Using ACLOUD/PASCAL Multiplatform Observations to Unravel the Role of Clouds and Aerosol Particles
in Arctic Amplification, Bulletin of the American Meteorological Society, 100, 841 – 871, https://doi.org/10.1175/BAMS-D-18-0072.1,
2019.

Westbrook, C. D. and Illingworth, A. J.: Evidence that ice forms primarily in supercooled liquid clouds at temperatures > -27°C, Geophysical
Research Letters, 38, https://doi.org/https://doi.org/10.1029/2011GL048021, 2011.

790 Wieder, J., Ihn, N., Mignani, C., Haarig, M., Bühl, J., Seifert, P., Engelmann, R., Ramelli, F., Kanji, Z. A., Lohmann, U., and Henneberger, J.: Retrieving ice-nucleating particle concentration and ice multiplication factors using active remote sensing validated by in situ observations, Atmospheric Chemistry and Physics, 22, 9767–9797, https://doi.org/10.5194/acp-22-9767-2022, 2022a.

Wieder, J., Mignani, C., Schär, M., Roth, L., Sprenger, M., Henneberger, J., Lohmann, U., Brunner, C., and Kanji, Z. A.: Unveiling atmospheric transport and mixing mechanisms of ice-nucleating particles over the Alps, Atmospheric Chemistry and Physics, 22, 3111–3130,
795 https://doi.org/10.5194/acp-22-3111-2022, 2022b.

Wolff, M. A., Isaksen, K., Petersen-Øverleir, A., Ødemark, K., Reitan, T., and Brækkan, R.: Derivation of a new continuous adjustment function for correcting wind-induced loss of solid precipitation: results of a Norwegian field study, Hydrology and Earth System Sciences, 19, 951–967, https://doi.org/10.5194/hess-19-951-2015, 2015.

Yang, F., Cantrell, W. H., Kostinski, A. B., Shaw, R. A., and Vogelmann, A. M.: Is Contact Nucleation Caused by Pressure Perturbation?,
800 Atmosphere, 11, https://doi.org/10.3390/atmos11010001, 2020.

Young, G., Connolly, P. J., Jones, H. M., and Choularton, T. W.: Microphysical sensitivity of coupled springtime Arctic stratocumulus to modelled primary ice over the ice pack, marginal ice, and ocean, Atmospheric Chemistry and Physics, 17, 4209–4227, https://doi.org/10.5194/acp-17-4209-2017, 2017.

Young, G., Lachlan-Cope, T., O'Shea, S. J., Dearden, C., Listowski, C., Bower, K. N., Choularton, T. W., and Gallagher, M. W.:
805 Radiative Effects of Secondary Ice Enhancement in Coastal Antarctic Clouds, Geophysical Research Letters, 46, 2312–2321, https://doi.org/https://doi.org/10.1029/2018GL080551, 2019.

Young, K. C.: The role of contact nucleation in ice phase initiation in clouds, Journal of Atmospheric Sciences, 31, 768–776, 1974.

Zhao, X., Liu, X., Phillips, V. T. J., and Patade, S.: Impacts of secondary ice production on Arctic mixed-phase clouds based on ARM observations and CAM6 single-column model simulations, Atmospheric Chemistry and Physics, 21, 5685–5703, https://doi.org/10.5194/acp-
810 21-5685-2021, 2021.